

Supplementary Information for

Highly inert Cu(II) complexes of C-aryl bifunctional cyclam-picolinates with remarkable ^{64}Cu -labeling and biodistribution

Julie Pineau,^a Luís M. P. Lima,^b Marie M. Le Roy,^a Séverine Marionneau-Lambot,^c Marie Cordier,^d Patricia Le Saëc,^c Jan Rijn Zeevaart,^e Cathryn H. S. Driver,^e Alain Faivre-Chauvet,^c Nathalie Le Bris,^{a,*} and Raphaël Tripier^{a,*}

a. Univ. Brest, CEMCA, UMR CNRS 6521, 6 Av. Victor le Gorgeu, 29200 Brest, France.

b. Univ. Nova de Lisboa, ITQB, Av. da República, 2780-157 Oeiras, Portugal.

c. Univ. Nantes, CRCI2NA, UMR INSERM 1307, UMR CNRS 6075, 8 Quai Moncousu, 44007 Nantes, France.

d. Univ. Rennes, ISCR, UMR CNRS 6226, 263 Av. Général Leclerc, 35700 Rennes, France.

e. South African Nuclear Energy Corporation, Radiochemistry and PreClinical Imaging Facility, Elias Motsoaledi Street, R104 Pelindaba, North West, 0240, South Africa.

Table of content

| | |
|---|----|
| Acknowledgements | 4 |
| Live subject statement | 4 |
| Generalities | 5 |
| Ligands and complexes syntheses and characterization | 6 |
| Figure S1. Synthetic pathway of precursor 6 | 6 |
| Figure S2. Synthetic pathway of ligands 8 and 10 | 7 |
| Figure S3. Synthetic pathway of the Cu(II) complexes 11 and 12 | 8 |
| Experimental protocols | 9 |
| NMR, IR and HRMS spectra of all compounds | 13 |
| Figure S4. ¹ H and ¹³ C-Jmod NMR spectra of compound 2 | 13 |
| Figure S5. HRMS (ESI ⁺) spectrum of compound 2 | 14 |
| Figure S6. IR spectrum of compound 2 | 15 |
| Figure S7: ¹ H and ¹³ C-Jmod NMR spectra of compound 3 | 16 |
| Figure S8. HRMS (ESI ⁺) spectrum of compound 3 | 17 |
| Figure S9. IR spectrum of compound 3 | 18 |
| Figure S10. ¹ H NMR spectrum of compound 5 | 19 |
| Figure S11. HRMS (ESI ⁺) spectrum of compound 5 | 20 |
| Figure S12. ¹ H and ¹³ C-Jmod NMR spectra of compound 6 | 21 |
| Figure S13. ¹ H and ¹³ C-Jmod NMR spectra of compound 7 | 22 |
| Figure S14. HRMS (ESI ⁺) spectrum of compound 7 | 23 |
| Figure S15. ¹ H and ¹³ C-Jmod NMR spectra of ligand H ₂ TE1PA-trz-prA.4HCl (8) | 24 |
| Figure S16. HRMS (ESI ⁺) spectrum of ligand H ₂ TE1PA-trz-prA.4HCl (8) | 25 |
| Figure S17. ¹ H NMR spectrum of compound 9 | 26 |
| Figure S18. ¹ H and ¹³ C-Jmod NMR spectra of ligand H ₂ CB-TE1PA-trz-prA.2HCl (10) | 27 |
| Figure S19. HRMS (ESI ⁺) spectrum of ligand H ₂ CB-TE1PA-trz-prA.2HCl (10) | 28 |
| Figure S20. HRMS (ESI ⁺) spectrum of complex [Cu(TE1PA-trz-prA)] (11) | 29 |
| Figure S21. HRMS (ESI ⁺) spectrum of complex [Cu(CB-TE1PA-trz-prA)] (12) | 30 |
| Thermodynamic equilibrium studies | 31 |
| Figure S22. Titration curves of H ₂ TE1PA-trz-prA and H ₂ CB-TE1PA-trz-prA | 32 |
| Table S1. Stepwise protonation constants of ligands 8 and 9 | 33 |
| Table S2. Overall, stepwise stability constants and pCu values for complexes 11 and 12 | 34 |

| | |
|---|----|
| Figure S23. Species distribution diagrams of complexes 11 and 12 | 34 |
| X-Ray diffraction determination of [Cu(CB-TE1PA-trz-prA)] | 35 |
| Figure S24. View of the crystal structures of the four complexes of [Cu(CB-TE1PA-trz-prA)] | 37 |
| Table S3. Crystallographic data of [Cu(CB-TE1PA-trz-prA)] (12) | 38 |
| Table S4. Selected bond lengths and angles of [Cu(CB-TE1PA-trz-prA)] (12) | 40 |
| Figure S25. UV and vis-NIR absorption spectra of complexes 11 and 12 | 40 |
| Table S5. UV-vis-NIR absorption parameters for complexes 11 and 12 | 41 |
| Figure S26. EPR spectra of complexes 11 and 12 | 41 |
| Table S6. Simulated EPR parameters for complexes 11 and 12 | 41 |
| Kinetic inertness studies | 42 |
| Figure S27. Plots of the acid-assisted dissociation of complexes 11 and 12 | 42 |
| Cyclic voltammetry studies | 43 |
| Figure S28. Cyclic voltammograms of complexes 11 and 12 | 43 |
| Table S7. Cyclic voltammetry parameters of complexes 11 and 12 | 44 |
| Radiolabeling studies | 45 |
| H₂CB-TE1PA-trz-prA: conjugation, radiolabeling and characterization | 45 |
| Figure S29. Determination of the number of chelates per antibody | 46 |
| Figure S30. HPLC profiles of the bioconjugates | 47 |
| Radiolabeling of H₂TE1PA-trz-prA | 48 |
| Figure S31. TLC-PET analysis after [⁶⁴ Cu]-labeling of H ₂ TE1PA-trz-prA | 48 |
| Figure S32. HPLC-radiochromatogram after ⁶⁴ Cu-labeling of H ₂ TE1PA-trz-prA | 49 |
| Figure S33. Gel filtration analysis of serum incubated with [⁶⁴ Cu][Cu(TE1PA-trz-prA)] | 49 |
| <i>In vivo</i> studies with [⁶⁴Cu][Cu(TE1PA-trz-prA)] and micro-PET imaging | 49 |
| Figure S34. Dynamic micro-PET images of BALB/c mice with [⁶⁴ Cu][Cu(TE1PA-trz-prA)] | 51 |
| Figure S35. Pharmacokinetic curves liver and kidneys from dynamic micro-PET images | 53 |
| Figure S36. Pharmacokinetic curves of bladder compared to liver and kidneys | 53 |
| Figure S37. Goodness of fit of biodistribution in liver, kidneys and bladder | 54 |
| Figure S38. Biodistribution of [⁶⁴ Cu][Cu(TE1PA-trz-prA)] and [⁶⁴ Cu][Cu(TE1PA)] ⁺ in BALB/c mice | 55 |
| References | 56 |

Acknowledgements

R.T. and N.L.B. acknowledge the Ministère de l'Enseignement Supérieur et de la Recherche and the Centre National de la Recherche Scientifique. J.P. is grateful to the Ligue contre le Cancer, the MAC-group (UBO) and the University of Cape Town for her PhD fellowship. M.C. thanks Thierry Roisnel for his participation in the collection of SCXRD data. L.M.P.L was financially supported by FCT - Fundação para a Ciência e a Tecnologia, I.P., through MOSTMICRO-ITQB R&D Unit (UIDB/04612/2020, UIDP/04612/2020) and LS4FUTURE Associated Laboratory (LA/P/0087/2020).

Live Subject Statement

All experiments were performed in compliance with the relevant laws and institutional guidelines. CEEA N°6 (Pays de la Loire, France) approved this research accredited by French Research Ministry under project #22764. Animals were housed in the UTE animal facility (University of Nantes, license no. B-44-278) under conventional conditions.

Generalities

Material and methods

Reagents used for synthesis were purchased from Acros Organics[®] or Sigma-Aldrich[®] and used without further purification. Ultrapure water was freshly obtained from a Milli-Q dispenser. A solvent purification system was used to dispense dry solvents before each reaction.

Spectroscopic Studies

¹H and ¹³C NMR spectra were recorded at the “Services communs” of the University of Brest on Bruker Avance 500 (500 MHz), Bruker Avance 400 (400 MHz) or Bruker AMX-3 300 (300 MHz) spectrometers. Coupling constants are given in hertz and chemical shifts in ppm.

EPR spectra of Cu(II) complexes were recorded at the “Services Communs” as well on a Bruker Elexsys 500 instrument, in a 0.5 mm capillary within a quartz tube, at 9.34 GHz (band X) using a complex concentration of ca. 1.0 mM. Simulations of the experimental spectra were performed using Easyspin¹ and Simultispin² software. Spectra were acquired in frozen DMF/H₂O (1:1) solutions at 140–160 K with a continuous-flow cryostat for liquid nitrogen, at a microwave power of 2.0 mW and a frequency of 9.5 GHz.

Absorption spectra of Cu(II) complexes, in aqueous solutions at neutral pH, were measured at 25 °C on PerkinElmer lambda 650 (UV) and Shimadzu UV-3100 (vis-NIR) spectrophotometers on Hellma 1400 μL quartz cuvettes with 1 cm optical path.

IR spectra of compounds **2**, **3** and **4** that contains azide or alkyne function were recorded at 25 °C on FT-IR Perkin Elmer spectrometer (ATR diamond).

Mass spectrometry

The high-resolution mass spectra of compounds were recorded at Institute of Organic and Analytic Chemistry (ICOA, Orleans, France) with a HRMS Q-ToF MaXis instrument, using ESI, APCI, APPI or nano-ESI for ionization. The low-resolution Mass Spectrometry analyses were performed at the “Services communs” of the University of Brest on a Waters Synapt XS, source ESI.

Ligands and complexes syntheses and characterization

The starting iodinated picolinate **1**³ as well as methyl 3-azidopropanoate **4**⁴ were obtained following previously reported procedures. The *C*-aryl-functionalized chelating unit **6** was synthesized in four steps from the iodinated picolinate **1**.

For that purpose, the protected alkyne derivative **2** was obtained by a Sonogashira coupling between the picolinate derivative **1** and TMS-ethyne in presence of Pd(PPh₃)₂Cl₂ and CuI as catalysts, at 50 °C for 16 hours. Compound **2** was isolated after a recrystallization from diethyl ether with 86% yield. This value is similar to those of the literature although purification on silica gel column is often carried out.^{3,5} The further removal of the TMS group with TBAF in THF led to the terminal alkyne **3** in 93% yield. A Copper(I)-Alkyne Azide Cycloaddition (CuAAC) between alkyne **3** and azide **4** was performed in a mixture of THF/H₂O (3:1) at room temperature for 1 hour in the presence of CuSO₄·5H₂O and sodium ascorbate. Compound **5** was obtained in a very high yield with no by-products. The hydroxyl group of derivative **5** was then successfully activated as a mesylate function under standard conditions⁶ to afford quasi-quantitatively compound **6** (Figure S1).

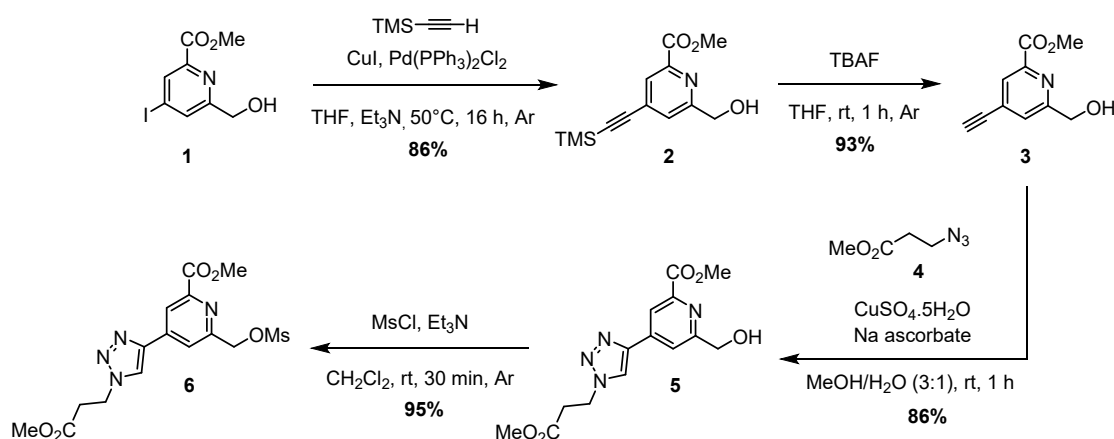


Figure S1. Synthesis of triazole-propionic acid-picolinate precursor **6**.

To access the attempted mono-*N*-alkylated cyclam **8**, the commercial triBoc-cyclam was reacted with the mesylated derivative **6** in the presence of K₂CO₃, in CH₃CN at reflux for three days. The crude product was purified by silica column chromatography to yield the pure alkylated triBoc-cyclam **7** with 75% yield. Boc groups as well as methyl ester functions of the alkylated derivative **7** were removed by treatment with a hydrochloric acid solution (3 M) under reflux for 16 hours. After precipitation in acetone, H₂TE1PA-trz-prA·4HCl **8** was obtained under as hydrochloride salt with a quasi-quantitative yield. The synthesis of the cross-bridged cyclam derivative **10** was performed in two steps from commercially cross-bridged cyclam (CB-cyclam). The alkylation with mesylate derivative **6** was carried out in CH₃CN at room temperature for 8 hours to afford compound **9** in 66% yield after silica column chromatography.

The use of a base was in this case not required here since the protonation of the free secondary amine function prevents the second alkylation. This selective mono-*N*-functionalization is due to the “proton sponge” behavior of the reinforced cyclam with a first protonation constant greater than 12. In the same way as for the previous ligand, compound **9** was hydrolyzed in a hydrochloric acid solution (3 M), under reflux for 16 hours. The addition of acetone allowed the precipitation of the desired H₂CB-TE1PA-trz-prA.2HCl **10** in its hydrochloride salt with a quasi-quantitative yield. The overall yield of the synthesis of compound **6** was 46% in 6 steps (Figure S2).

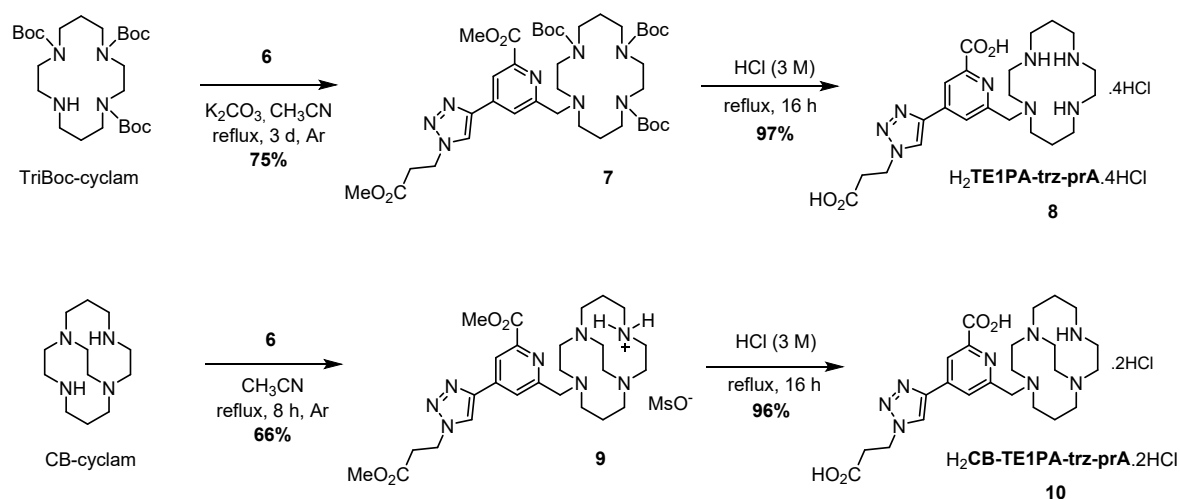


Figure S2. Syntheses of H₂TE1PA-trz-prA.4HCl **8** and H₂CB-TE1PA-trz-prA.2HCl **10** from mesylated reagent **6** and, respectively, triBoc-cyclam and CB-cyclam.

The ligands under their hydrochloride salts **8** or **10** (1 equiv) were dissolved in water ($C = 0.05$ M) and the pH of the solution was adjusted to 6.0–7.0 with aqueous KOH solution before the addition of 1.1 equiv of Cu(ClO₄)₂·6H₂O. The reaction was refluxed and the pH was adjusted again to 6–7 by addition of 1 M aqueous KOH solution. The mixture was stirred for 16 h under reflux (Figure S3). After cooling to room temperature, solid impurities were filtered off and the solution was evaporated under vacuum. The residue was purified on reverse phase C18 flash chromatography with H₂O/MeOH (100:0 to 95:5). The corresponding complexes [Cu(TE1PA-trz-prA)] **11** and [Cu(CB-TE1PA-trz-prA)] **12** were isolated with 90% and 81% yield respectively.

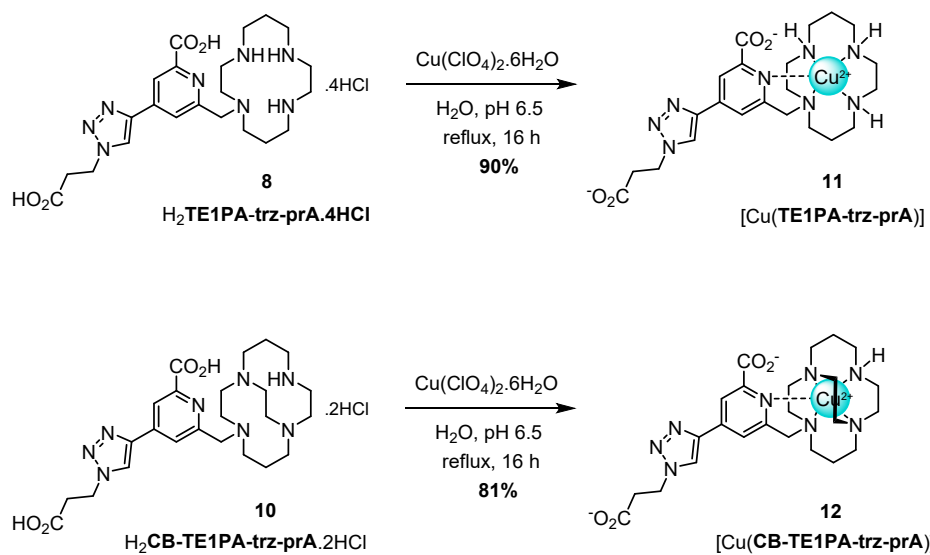


Figure S3. Reaction of ligands **8** and **10** with $\text{Cu}(\text{ClO}_4)_2 \cdot 6\text{H}_2\text{O}$ at pH 6.5 leading respectively to $[\text{Cu}(\text{TE1PA-trz-prA})]$ (**11**) and $[\text{Cu}(\text{CB-TE1PA-trz-prA})]$ (**12**).

Experimental protocols

Compound 2: Trimethylsilylacetylene (1.30 mL, 9.44 mmol, 1.5 equiv) was added to a solution of compound **1**³ (1.85 g, 6.31 mmol) in a mixture of THF (25 mL) and Et₃N (4 mL, 28.33 mmol, 4.5 equiv). The solution was degassed three times and Pd(PPh₃)₂Cl₂ (133 mg, 0.19 mmol) and CuI (72 mg, 0.38 mmol) were added. The reaction was stirred at 55 °C for 16 h. After cooling to room temperature, the mixture was filtered over Celite® and the solvent was evaporated *in vacuo*. The residue was dissolved in CHCl₃ (50 mL) and washed with NH₄Cl (3 × 40 mL), H₂O (2 × 40 mL) and brine (1 × 40 mL). The organic layer was dried over MgSO₄, filtered and concentrated *in vacuo*. The crude solid was purified by recrystallization with hot Et₂O to give compound **2** as white crystals (1.43 g, 86%). ¹H NMR (300 MHz, CDCl₃, 25 °C) δ (ppm): 8.02 (s, 1H, CH_{Ar}), 7.56 (s, 1H, CH_{Ar}), 4.82 (s, 2H, CH₂α-OH), 3.98 (s, 3H, O-CH₃), 3.03 (br, 1H, OH), 0.26 (s, 9H, Si(CH₃)₃). ¹³C Jmod NMR (75 MHz, CDCl₃, 25 °C) δ (ppm): 165.2 (CO), 160.8 (C_{ipso}), 147.2 (C_{ipso}), 133.4 (C_{ipso}), 126.2 (CH_{Ar}), 126.0 (CH_{Ar}), 101.8 (C_{sp}), 101.3 (C_{sp}), 64.6 (CH₂α-OH), 53.1 (O-CH₃), 0.3 ((Si-CH₃)₃). **ESI-HRMS:** *m/z* calcd for [C₁₃H₁₈NO₃Si]⁺ 264.1050 found [M+H]⁺ 264.1055; calcd for [C₁₃H₁₇NNaO₃Si]⁺ 286.0870 found [M+Na]⁺ 286.0871. **IR** ν (cm⁻¹): 3438 (OH), 2167 (C≡C), 1728 (C=O).

Compound 3: Tetrabutylammonium fluoride (1 M in THF) (1.97 mL, 1.97 mmol, 1.1 equiv) was added at 0 °C under an argon atmosphere to a solution of compound **2** (473 mg, 1.79 mmol) in dry THF (9 mL). The mixture was stirred for 1 h at room temperature and then quenched by addition of H₂O (15 mL) and extracted with CH₂Cl₂ (4 × 20 mL). The combined organic layers were washed with NaHCO₃ (2 × 50 mL), H₂O (2 × 50 mL) and brine (1 × 50 mL) and dried over MgSO₄. After filtration and evaporation of the solvent, compound **3** was obtained without any further purification to yield a yellowish powder (319 mg, 93%). ¹H NMR (400 MHz, CDCl₃, 25 °C) δ (ppm): 8.05 (s, 1H, CH_{Ar}), 7.61 (s, 1H, CH_{Ar}), 4.85 (s, 2H, CH₂α-OH), 3.98 (s, 3H, CH₃-O), 3.37 (s, 1H, ≡CH). ¹³C Jmod NMR (75 MHz, CDCl₃, 25 °C) δ (ppm): 165.1 (CO), 161.0 (C_{ipso}), 147.4 (C_{ipso}), 132.5 (C_{ipso}), 126.4 (x2) (CH_{Ar}), 83.3 (≡CH), 80.4 (C_{sp}), 64.6 (CH₂α-OH), 53.2 (O-CH₃). **ESI-HRMS:** *m/z* calcd for [C₁₀H₁₀NO₃]⁺ 192.0655 found [M+H]⁺ 192.0655; calcd for [C₁₀H₉NNaO₃]⁺ 214.0475 found [M+Na]⁺ 214.0474. **IR** ν (cm⁻¹): 3400 (OH), 3224 (C-H alkyne), 2108 (C≡CH), 1745 (C=O).

Compound 5: Alkyne **3** (146 mg, 0.764 mmol) and azide **4**⁴ (101 mg, 0.779 mmol, 1.02 equiv) were dissolved in MeOH (6 mL). A solution of CuSO₄·5H₂O (9.5 mg, 0.038 mmol, 0.05 equiv) in H₂O (1 mL) and a solution of sodium ascorbate (30 mg, 0.153 mmol, 0.20 equiv) in H₂O (1 mL) were added. The deep orange solution was stirred at room temperature for 1 h and turned yellow. The MeOH solvent was removed *in vacuo* and the aqueous solution was extracted with CH₂Cl₂ (3 × 3 mL). Organic layers were washed with H₂O (2 × 12 mL) and brine (2 × 12 mL), dried over MgSO₄, filtered and concentrated *in vacuo* to afford compound **5** as a yellowish powder (232 mg, 95%). ¹H NMR (300 MHz, CDCl₃, 25 °C) δ (ppm): 8.36 (s, 1H, CH_{Ar}),

8.14 (s, 1H, CH_{Ar} trz), 8.03 (s, 1H, CH_{Ar} pico), 4.90 (s, 2H, $CH_2\alpha$ -OH), 4.74 (t, 2H, $J = 6.2$ Hz, $CH_2\alpha$ -trz), 4.00 (s, 3H, O- CH_3 pico), 3.71 (s, 3H, O- CH_3 chain), 3.03 (t, 2H, $J = 6.2$ Hz, 2H, $CH_2\alpha$ - CO_2CH_3). **^{13}C Jmod NMR** (125 MHz, $CDCl_3$, 25 °C) δ (ppm): 171.1 (CO chain), 165.4 (CO pico), [161.8, 147.6, 144.4, 140.0] (C_{ipso} pico, C_{ipso} trz), [123.2, 120.2, 119.9] (CH_{Ar} pico, CH_{Ar} trz), 64.7 ($CH_2\alpha$ -OH), [53.0, 52.3] (O CH_3 chain, O- CH_3 pico), 45.9 ($CH_2\alpha$ -trz), 34.3 ($CH_2\alpha$ - CO_2CH_3). **ESI-HRMS**: m/z calcd for $[C_{14}H_{17}N_4O_5]^+$ 321.1193 found $[M+H]^+$ 321.1193.

Compound 6: Mesyl chloride (32 μ L, 0.414 mmol, 1.3 equiv) was added dropwise under an argon atmosphere to a solution of compound **5** (102 mg, 0.318 mmol) in CH_2Cl_2 (16 mL) and triethylamine (67 μ L, 0.478 mmol, 1.5 equiv). The solution was stirred at room temperature for 30 min with TLC monitoring. The solution was washed with $NaHCO_3$ (3×12 mL), H_2O (3×12 mL) and brine (2×12 mL). The organic layer was dried over $MgSO_4$, filtered off and concentrated *in vacuo* to give compound **6** as a yellowish foam (121 mg, 95%). $R_f = 0.56$ (SiO_2 , AcOEt 100 %). **1H NMR** (400 MHz, $CDCl_3$, 25 °C) δ (ppm): 8.48 (d, 1H, $J = 1.3$ Hz, CH_{Ar} pico), 8.18 (s, 1H, CH_{Ar} trz), 8.11 (d, 1H, $J = 1.3$ Hz, CH_{Ar} pico), 5.46 (s, 2H, $CH_2\alpha$ -OMs), 4.75 (t, 2H, $J = 6.2$ Hz, $CH_2\alpha$ -trz), 4.02 (s, 3H, O- CH_3 pico), 3.72 (s, 3H, O- CH_3 chain), 3.18 (s, 3H, CH_3 -OMs), 3.05 (t, $J = 6.2$ Hz, 2H, $CH_2\alpha$ - CO_2CH_3). **^{13}C Jmod NMR** (100 MHz, $CDCl_3$, 25 °C): δ (ppm) 170.9 (CO chain), 165.0 (CO pico), [155.1, 148.4, 143.8, 140.7] (C_{ipso} pico, C_{ipso} trz), [123.3, 121.1, 120.9] (CH_{Ar} pico, CH_{Ar} trz), 70.9 ($CH_2\alpha$ -OMs), [53.0, 52.2] (O- CH_3 chain, O- CH_3 pico), 45.9 ($CH_2\alpha$ -trz), 38.0 (CH_3 -OMs), 34.1 ($CH_2\alpha$ - CO_2CH_3).

Compound 7: Mesyl compound **6** (297 mg, 0.745 mmol, 1.1 equiv) dissolved in dry CH_3CN (10 mL) was added to a solution of triBoc cyclam (339 mg, 0.677 mmol) in dry CH_3CN (25 mL). K_2CO_3 (936 mg, 6.771 mmol, 10 equiv) was added and the solution was stirred at reflux under an argon atmosphere for 4 days. The solution was cooled down to room temperature and filtrated off to remove K_2CO_3 salts. After evaporation of the filtrate, the residue was dissolved in $CHCl_3$ and the solution was filtered again to remove the remaining K_2CO_3 . The crude product was purified by chromatographic silica column eluted with CH_2Cl_2 /AcOEt (90:10 to 50:50) to give compound **7** as a white foam (408 mg, 75%). **1H NMR** (500 MHz, CD_3CN , 70 °C) δ (ppm): 8.45 (s, 1H, CH_{Ar} trz), 8.36 (s, 1H, CH_{Ar} pico), 8.02 (s, 1H, CH_{Ar} pico), 4.72 (t, 2H, $J = 6.7$ Hz, $CH_2\alpha$ -trz), 3.94 (s, 3H, O- CH_3 pico), 3.77 (s, 2H, CH_2 pico), 3.67 (s, 3H, O- CH_3 chain), 3.43-3.28 (m, 12H, $CH_2\alpha$ -N), 3.04 (t, 2H, $J = 6.7$ Hz, $CH_2\alpha$ - CO_2CH_3), 2.71-2.67 (m, 2H, $CH_2\alpha$ -N), 2.56-2.51 (m, 2H, $CH_2\alpha$ -N), 1.91-1.84 (m, 2H, $CH_2\beta$ -N), 1.78-1.71 (m, 2H, $CH_2\beta$ -N), 1.45 (s, 9H, CH_3 Boc), 1.41 (s, 9H, CH_3 Boc), 1.27 (s, 9H, CH_3 Boc). **^{13}C Jmod NMR** (125 MHz, CD_3CN , 70 °C) δ (ppm): 172.0 (CO chain), 166.9 (CO pico), 162.6 (C_{ipso}), [157.0, 156.6 (x2)] (CO Boc), [149.7, 145.5, 141.2] (C_{ipso}), 124.5 (CH_{Ar} trz), 123.6 (CH_{Ar} pico), 120.7 (CH_{Ar} pico), [80.3, 80.1, 80.0] (C_q Boc), 62.4 (CH_2 pico), [55.8, 53.9, 48.9, 48.8, 48.4, 48.3, 48.1] ($CH_2\alpha$ -N) [53.2, 52.7] (O- CH_3 chain, O- CH_3 pico), 47.2 ($CH_2\alpha$ -trz), 35.2 ($CH_2\alpha$ - CO_2CH_3), 30.0 ($CH_2\beta$ -N), [29.0 (x2), 28.9] (CH_3 Boc), 28.3 ($CH_2\beta$ -N). **ESI-HRMS**:

m/z calcd for $[C_{39}H_{63}N_8O_{10}]^+$ 803.4662 found $[M+H]^+$ 803.4653; calcd for $[C_{39}H_{62}N_8NaO_{10}]^+$ 825.4481 found $[M+Na]^+$ 825.4474.

H₂TE1PA-trz-prA.4HCl (8): Compound **7** (289 mg, 0.360 mmol) was dissolved in 3 M HCl (4 mL) and the solution was refluxed for 16 h. Excess of HCl was evaporated under reduced pressure and the crude product was purified by precipitations in H₂O/acetone to yield **8** as a white powder (216 mg, 97%). **¹H NMR** (500 MHz, D₂O, 25 °C) δ (ppm): 8.51 (s, 1H, CH_{Ar} trz), 8.10 (s, 1H, CH_{Ar} pico), 7.88 (s, 1H, CH_{Ar} pico), 4.68 (t, 2H, $J = 6.3$ Hz, CH₂ α -trz), 4.33 (s, 2H, CH₂ pico), 3.62-3.53 (m, 6H, CH₂ α -N), 3.48-3.33 (m, 6H), 3.29-3.24 (m, 2H, CH₂ α -N), 3.23-3.18 (m, 2H, CH₂ α -N), 3.04 (t, 2H, $J = 6.3$ Hz, CH₂ α -CO₂H), 2.31-2.23 (m, 2H, CH₂ β -N), 2.15-2.07 (m, 2H, CH₂ β -N). **¹³C Jmod NMR** (125 MHz, D₂O, 25 °C) δ (ppm): 174.4 (CO chain), 166.2 (CO pico), [155.9, 147.4, 143.1, 141.4] (C_{ipso} pico, C_{ipso} trz), 125.2 (CH_{Ar} trz), [122.6, 120.8] (CH_{Ar} pico), 57.5 (CH₂ pico), [51.5, 48.3] (CH₂ α -N), 46.2 (CH₂ α -trz), [42.2, 42.1, 41.9, 41.1, 39.9, 38.3] (CH₂ α -N), 33.8 (CH₂ α -CO₂H), [21.2, 19.8] (CH₂ β -N). **ESI-HRMS:** m/z calcd for $[C_{22}H_{35}N_8O_4]^+$ 475.2778 found $[M+H]^+$ 475.2776; calcd for $[C_{22}H_{36}N_8O_4]^{2+}$ 238.1424 found $[M+2H]^{2+}$ 238.1429.

Compound 9: To a solution of cross-bridged cyclam (88 mg, 0.359 mmol) in dry CH₃CN (126 mL), a solution of compound **6** (136 mg, 0.341, 0.95 equiv) in dry CH₃CN (10 mL) was added dropwise over a period of 8 h at room temperature and then the mixture was stirred for additional 8 h. The solvent was removed under reduced pressure and the residue was purified on silica flash chromatography eluted with CH₂Cl₂/MeOH (100:0 to 85:15) to afford compound **9** as a yellow foam (148 mg, 66%). **¹H NMR** (500 MHz, CD₃OD, 25 °C) δ (ppm): 8.74 (s, 1H, CH_{Ar} trz), 8.57 (s, 1H, CH_{Ar} pico), 8.10 (s, 1H, CH_{Ar} pico), 4.78 (t, 2H, $J = 6.5$ Hz, CH₂ α -trz), 4.23 (d, 1H, $J = 12.6$ Hz, CH₂ pico), 4.07 (s, 3H, O-CH₃ pico), 3.69 (s, 3H, O-CH₃ chain), 3.66-3.57 (m, 1H), 3.50 (d, 1H, $J = 12.6$ Hz, CH₂ pico), 3.20-3.12 (m, 2H), 3.09 (t, 2H, $J = 6.5$ Hz, CH₂ α -CO₂CH₃), 3.07-2.95 (m, 3H), 2.91-2.71 (m, 6H), 2.69 (s, 3H, CH₃-OMs), 2.68-2.46 (m, 6H), 2.07-1.96 (m, 1H, CH₂ β -N), 1.78-1.67 (m, 1H, CH₂ β -N), 1.66-1.55 (m, 1H, CH₂ β -N), 1.07-0.95 (m, 1H, CH₂ β -N).

H₂CB-TE1PA-trz-prA.2HCl (10): Compound **9** (148 mg, 0.232 mmol) was dissolved in 3 M HCl (3 mL) and the solution was refluxed for 16 h. Excess of HCl was evaporated under reduced pressure and the crude product was purified by precipitations in H₂O/acetone to yield **10** as a white powder (130 mg, 96%). **¹H NMR** (500 MHz, D₂O, 25 °C) δ (ppm): 8.47 (s, 1H, CH_{Ar} trz), 8.29 (s, 1H, CH_{Ar} pico), 7.87 (s, 1H, CH_{Ar} pico), 4.78 (d, 1H, $J = 13.5$ Hz, CH₂ pico), 4.66 (t, 2H, $J = 6.7$ Hz, CH₂ α -trz), 4.04 (d, 1H, $J = 13.5$ Hz, CH₂ pico), 3.93-3.84 (m, 1H), 3.64-3.00 (m, 12H), 2.94-2.85 (m, 1H), 2.84-2.76 (m, 4H, CH₂ α -CO₂H, CH₂ α -N), 2.69-2.56 (m, 3H), 2.50-2.40 (m, 1H), 2.39-2.24 (m, 2H), 1.82-1.70 (m, 1H, CH₂ β -N), 1.63-1.48 (m, 1H, CH₂ β -N). **¹³C Jmod NMR** (125 MHz, D₂O, 25 °C) δ (ppm): 180.5 (CO chain), 174.3 (CO pico), [158.7, 153.6, 146.5, 143.2] (C_{ipso} pico, C_{ipso} trz), 127.2 (CH_{Ar} trz), 126.4 (CH_{Ar} pico), 123.5

(CH_{Ar} pico), 61.3, 60.6, 59.7 (CH₂ pico), 58.2, 57.3, 56.3, 52.7, 52.4, 51.9, 50.8 (CH₂α-trz), 49.3, 44.6, 40.1 (CH₂α-CO₂H), [21.3, 21.1] (CH₂β-N). **ESI-HRMS:** *m/z* calcd for [C₂₄H₃₇N₈O₄]⁺ 501.2932 found [M+H]⁺ 501.2926; calcd for [C₂₄H₃₈N₈O₄]²⁺ 251.1502 found [M+2H]²⁺ 251.1505.

[Cu(**TE1PA-trz-prA**)] **11:** The complex was obtained as a violet powder (19 mg, 90%). **ESI-HRMS:** *m/z* calcd for [C₂₂H₃₃CuN₈O₄]⁺ 536.1915 found [M+H]⁺ 536.1919; calcd for [C₂₂H₃₄CuN₈O₄]²⁺ 268.5994 found [M+2H]²⁺ 268.5999.

[Cu(**CB-TE1PA-trz-prA**)] **12:** The complex was obtained as a blue powder (17 mg, 81%). **ESI-HRMS:** *m/z* calcd for [C₂₄H₃₅CuN₈O₄]⁺ 562.2072 found [M+H]⁺ 562.2077; calcd for [C₂₄H₃₆CuN₈O₄]²⁺ 281.6072 found [M+2H]²⁺ 281.6076.

NMR, IR and HRMS spectra of compounds (2 to 10) and Cu(II)-complexes (11 and 12)

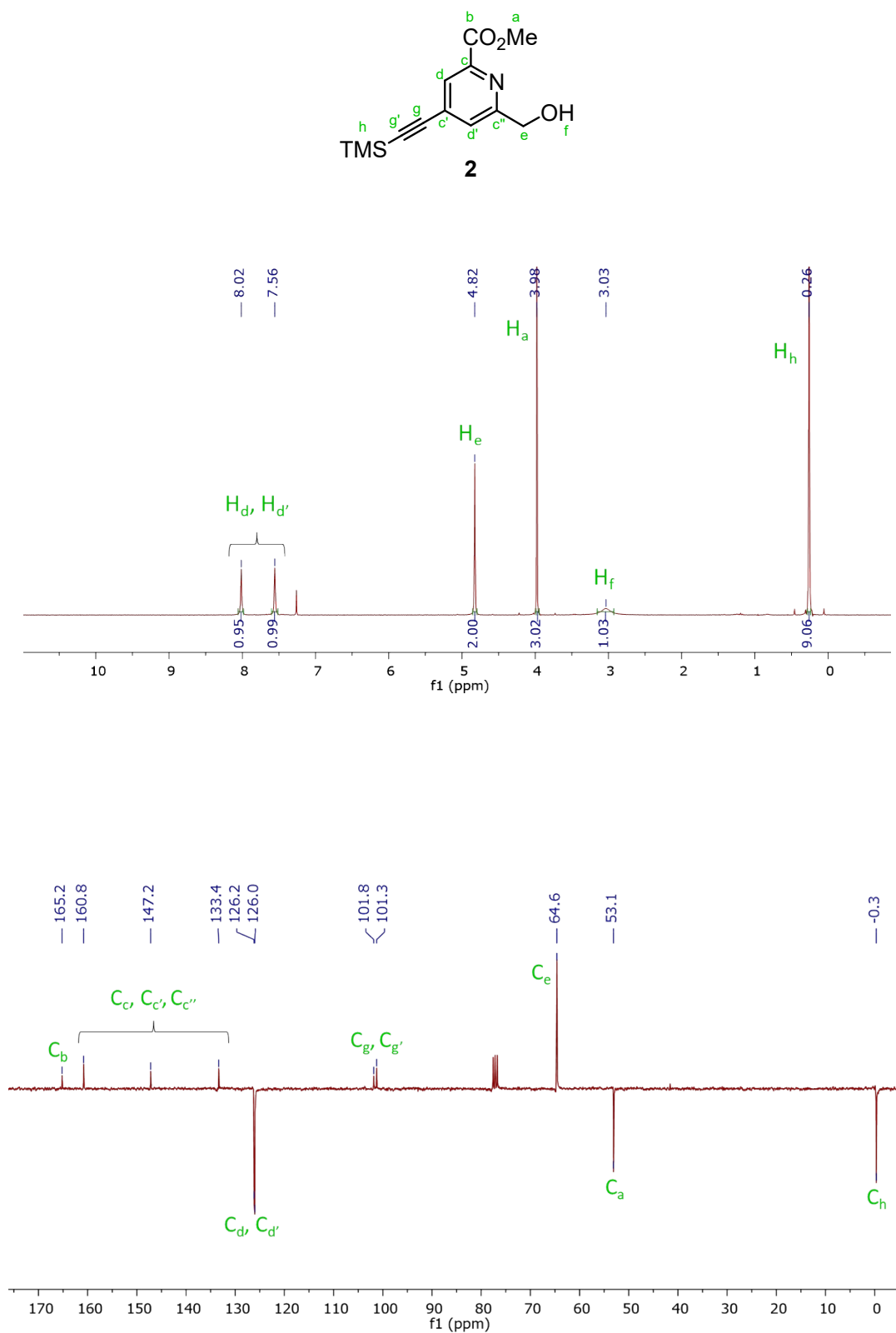
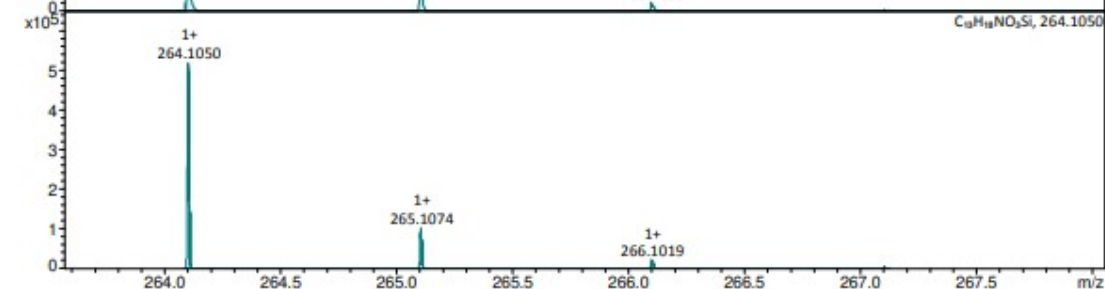
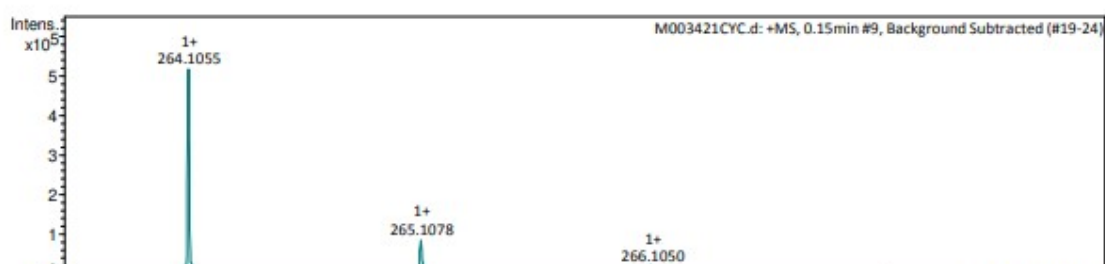
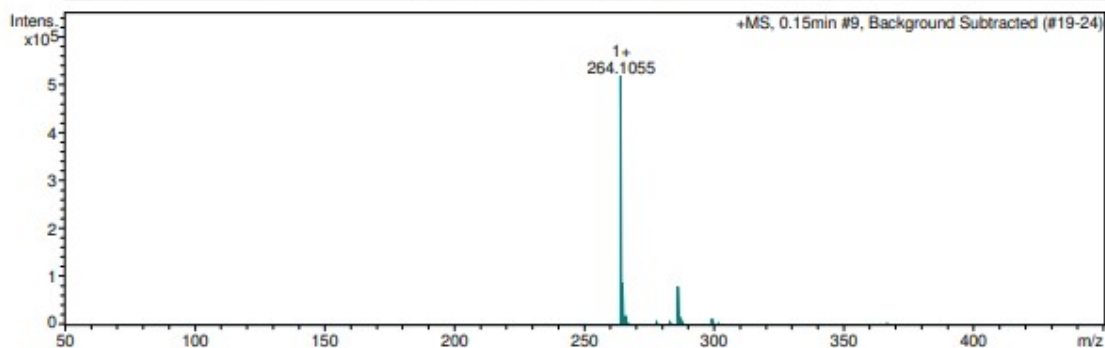


Figure S4. ¹H (300 MHz, CDCl₃, 25 °C) and ¹³C-Jmod (75 MHz, CDCl₃, 25 °C) NMR spectra of compound **2**.

| | | | |
|----------------------|----------------|-------------------|---------------------|
| Analysis Info | | Acquisition Date | 13/06/2019 22:34:07 |
| Sample Name | MLR 008 | Instrument / Ser# | maXis 266638.10141 |
| Analysis Name | M003421Cyc.d | Method | positif.m |

| | | | | | |
|------------------------------|----------|-----------------------|-----------|----------------|-----------|
| Acquisition Parameter | | | | | |
| Source Type | ESI | Ion Polarity | Positive | Set Nebulizer | 0.6 Bar |
| Scan Begin | 75 m/z | Set Capillary | 4500 V | Set Dry Heater | 201 °C |
| Scan End | 2500 m/z | Set Collision Cell RF | 900.0 Vpp | Set Dry Gas | 7.0 l/min |



| Meas. m/z | z | # | Ion Formula | m/z | err [ppm] | mSigma | rdb | e ⁻ | Conf |
|------------|----|---|--|------------|-----------|--------|-----|----------------|------|
| 264.105471 | 1+ | 1 | C ₁₃ H ₁₈ NO ₃ Si | 264.105046 | -1.6 | 17.3 | 7.0 | even | |
| 286.087066 | 1+ | 1 | C ₁₃ H ₁₇ NNaO ₃ Si | 286.086991 | -0.3 | 11.8 | 7.0 | even | |

Figure S5. HRMS (ESI⁺) spectrum of compound **2**.

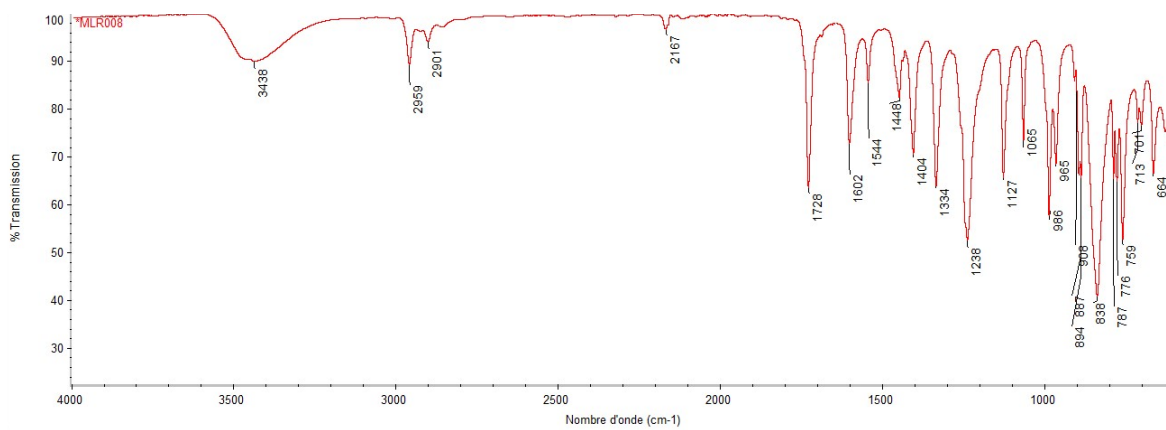


Figure S6. IR spectrum of compound 2.

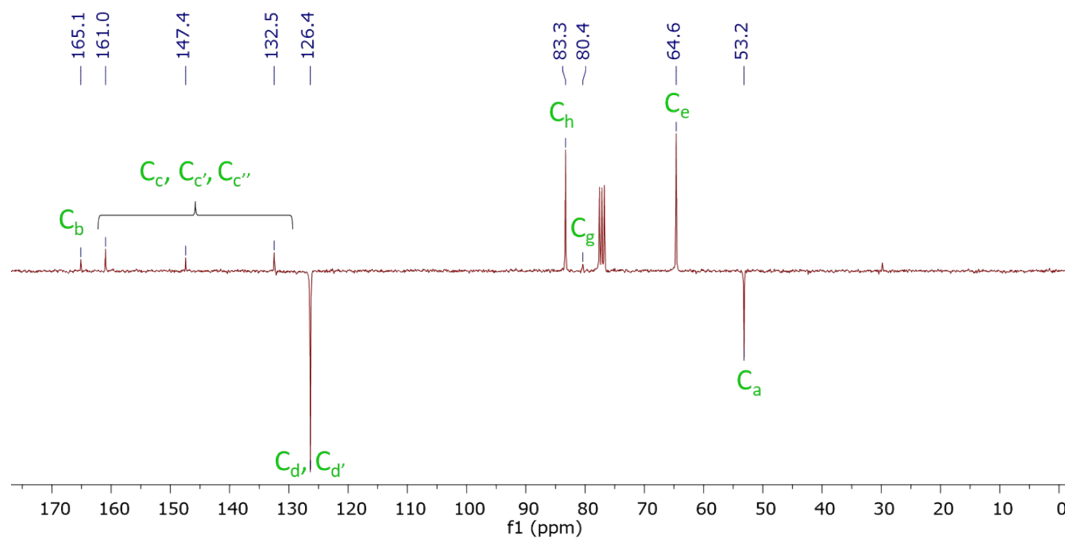
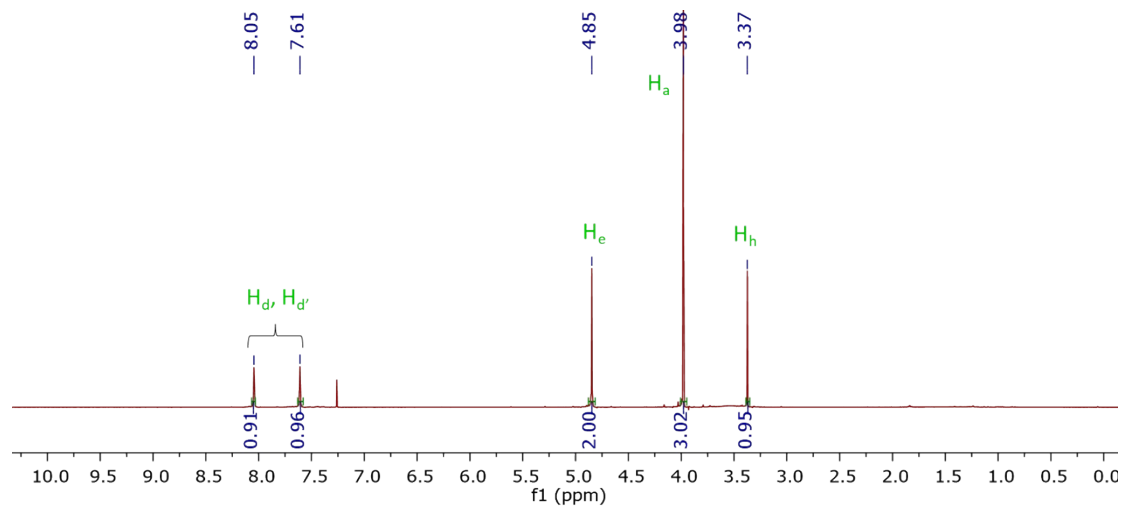
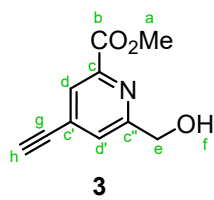
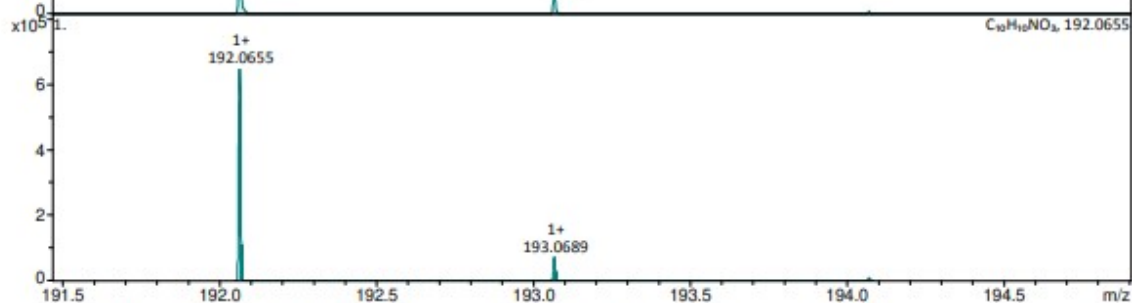
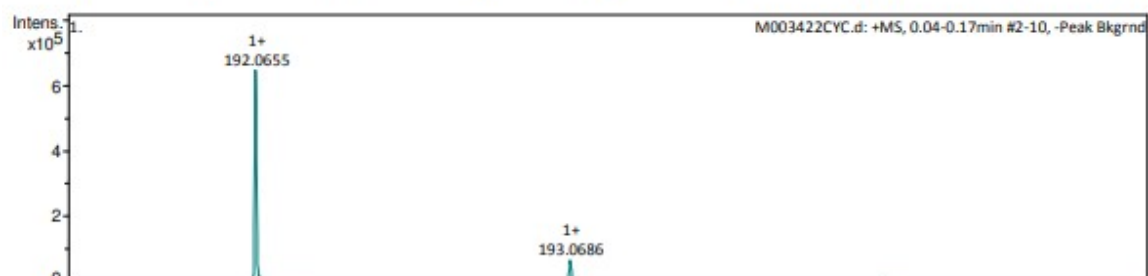
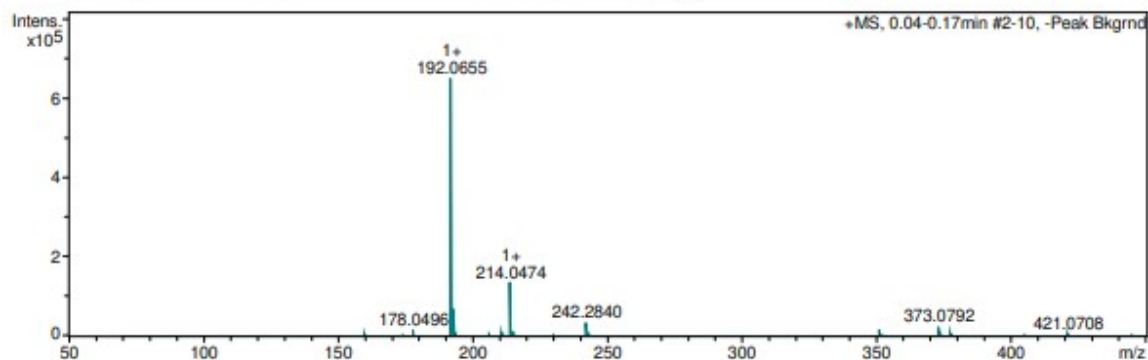


Figure S7. ^1H (400 MHz, CDCl_3 , 25 °C) and ^{13}C -Jmod (75 MHz, CDCl_3 , 25 °C) NMR spectra of compound **3**.

| | | | |
|----------------------|--------------|-------------------|---------------------|
| Analysis Info | | Acquisition Date | 13/06/2019 22:35:37 |
| Sample Name | MLR 009 | Instrument / Ser# | maXis 266638.10141 |
| Analysis Name | M003422CYC.d | Method | positif.m |

| | | | | | |
|------------------------------|----------|-----------------------|-----------|----------------|-----------|
| Acquisition Parameter | | | | | |
| Source Type | ESI | Ion Polarity | Positive | Set Nebulizer | 0.6 Bar |
| Scan Begin | 75 m/z | Set Capillary | 4500 V | Set Dry Heater | 201 °C |
| Scan End | 2500 m/z | Set Collision Cell RF | 900.0 Vpp | Set Dry Gas | 7.0 l/min |



| Meas. m/z | z | # | Ion Formula | m/z | err [ppm] | mSigma | rdb | e ⁻ | Conf |
|------------|----|---|-------------|------------|-----------|--------|-----|----------------|------|
| 192.065515 | 1+ | 1 | C10H10NO3 | 192.065520 | 0.0 | 5.1 | 7.0 | even | |
| 214.047373 | 1+ | 1 | C10H9NNaO3 | 214.047464 | 0.4 | 1.5 | 7.0 | even | |

Figure S8. HRMS (ESI⁺) spectrum of compound **3**.

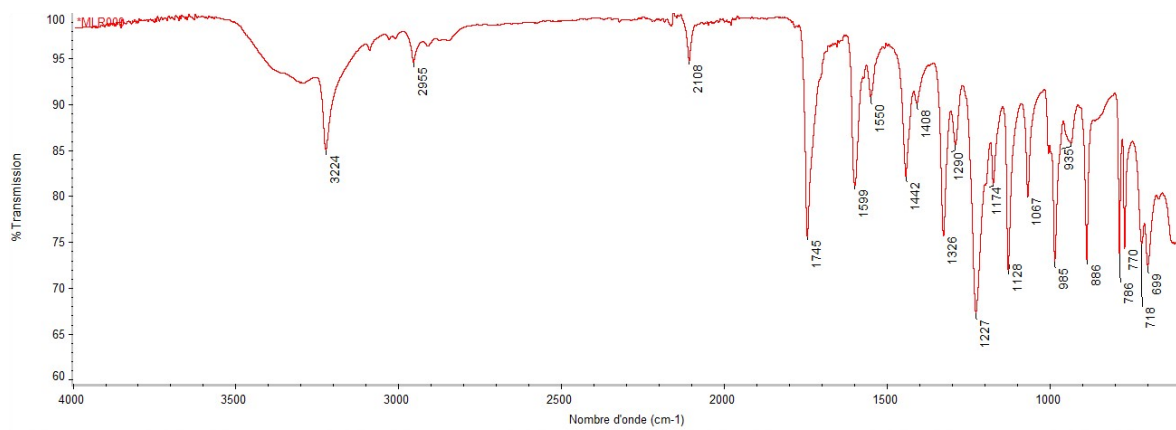


Figure S9. IR spectrum of compound **3**.

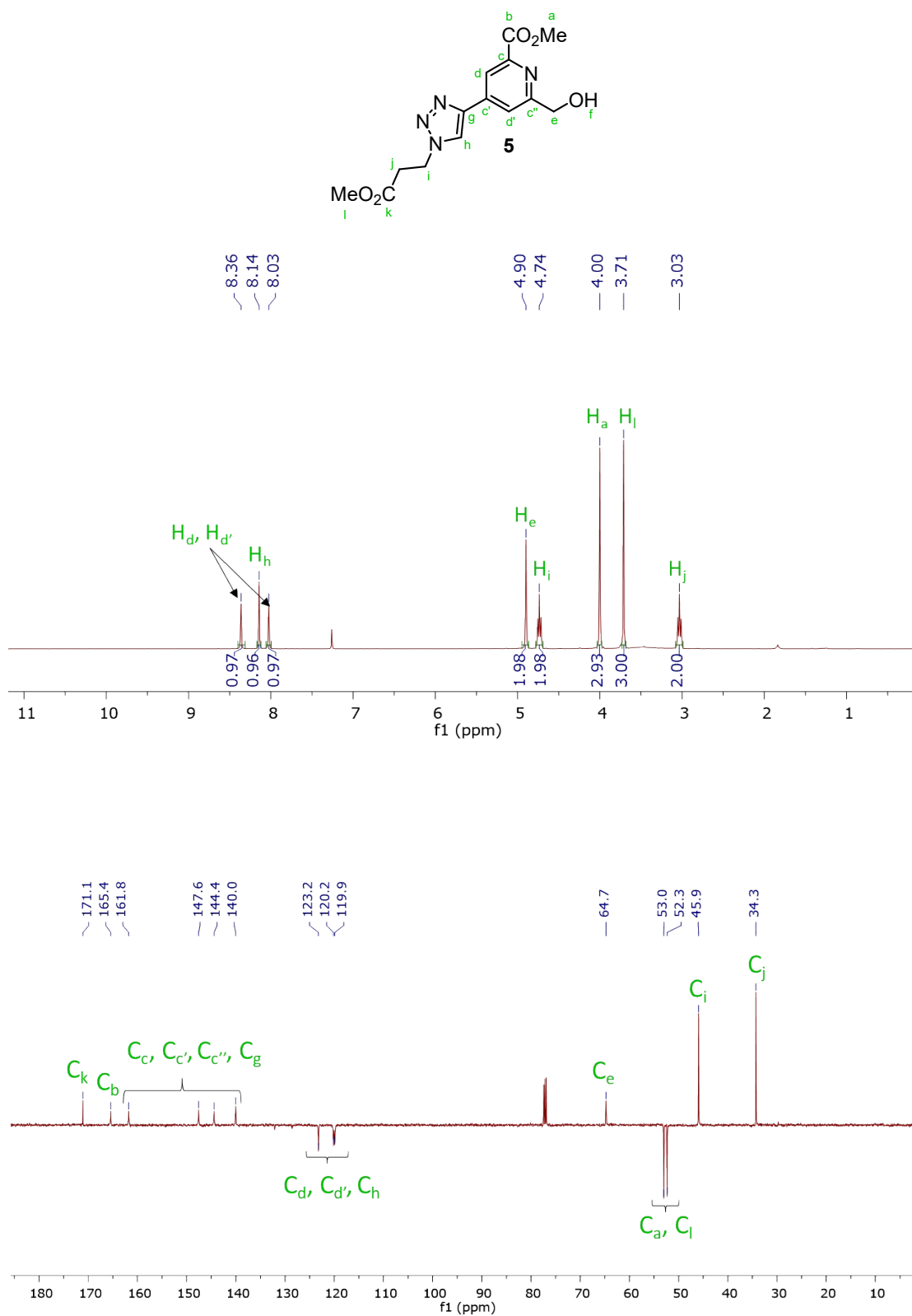
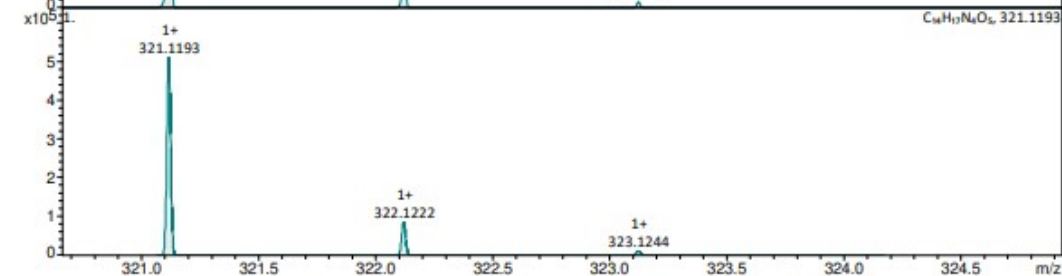
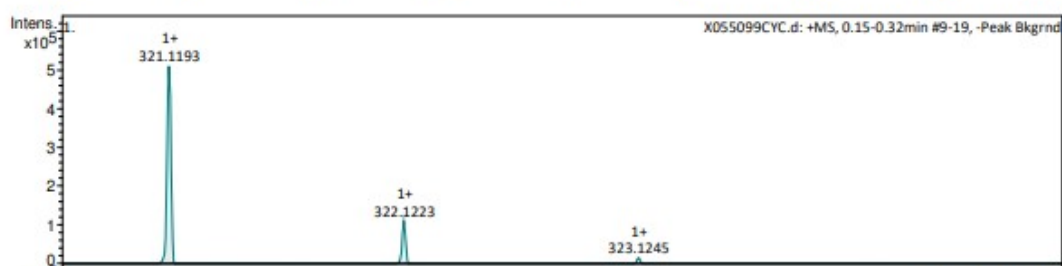
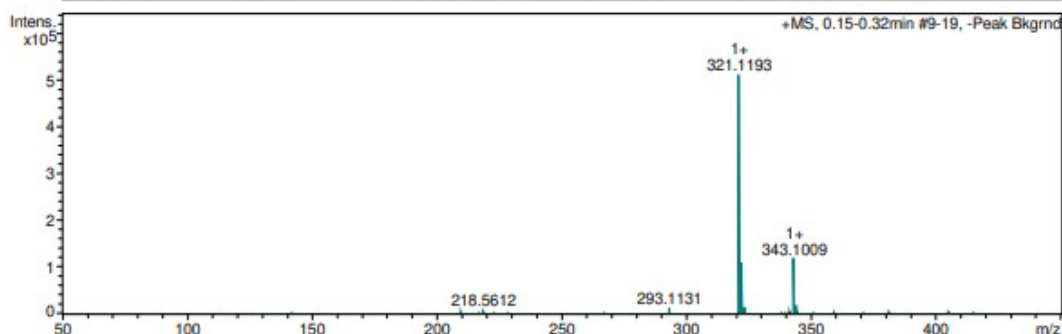


Figure S10. ¹H (300 MHz, CDCl₃, 25 °C) and ¹³C-Jmod (125 MHz, CDCl₃, 25 °C) NMR spectra of compound **5**.

| | | | |
|----------------------|--------------|-------------------|---------------------|
| Analysis Info | | Acquisition Date | 26/02/2020 11:19:22 |
| Sample Name | JP96 | Instrument / Ser# | maXis 255552.00086 |
| Analysis Name | X055099CVC.d | Method | Positif.m |

| | | | | | |
|------------------------------|----------|-----------------------|------------|----------------|-----------|
| Acquisition Parameter | | | | | |
| Source Type | ESI | Ion Polarity | Positive | Set Nebulizer | 0.6 Bar |
| Scan Begin | 50 m/z | Set Capillary | 4500 V | Set Dry Heater | 200 °C |
| Scan End | 3000 m/z | Set Collision Cell RF | 1800.0 Vpp | Set Dry Gas | 7.0 l/min |



| Meas. m/z | z | # | Ion Formula | m/z | err [ppm] | mSigma | rdB | e ⁻ | Conf |
|------------|----|---|---|------------|-----------|--------|-----|----------------|------|
| 293.113058 | 1+ | 1 | C ₁₄ H ₁₇ N ₂ O ₅ | 293.113198 | 0.5 | 14.9 | 8.0 | even | |
| 321.119300 | 1+ | 1 | C ₁₄ H ₁₇ N ₄ O ₅ | 321.119346 | 0.1 | 27.0 | 9.0 | even | |
| 343.100916 | 1+ | 1 | C ₁₄ H ₁₆ N ₄ NaO ₅ | 343.101290 | 1.1 | 7.7 | 9.0 | even | |

Figure S11. HRMS (ESI⁺) spectrum of compound **5**.

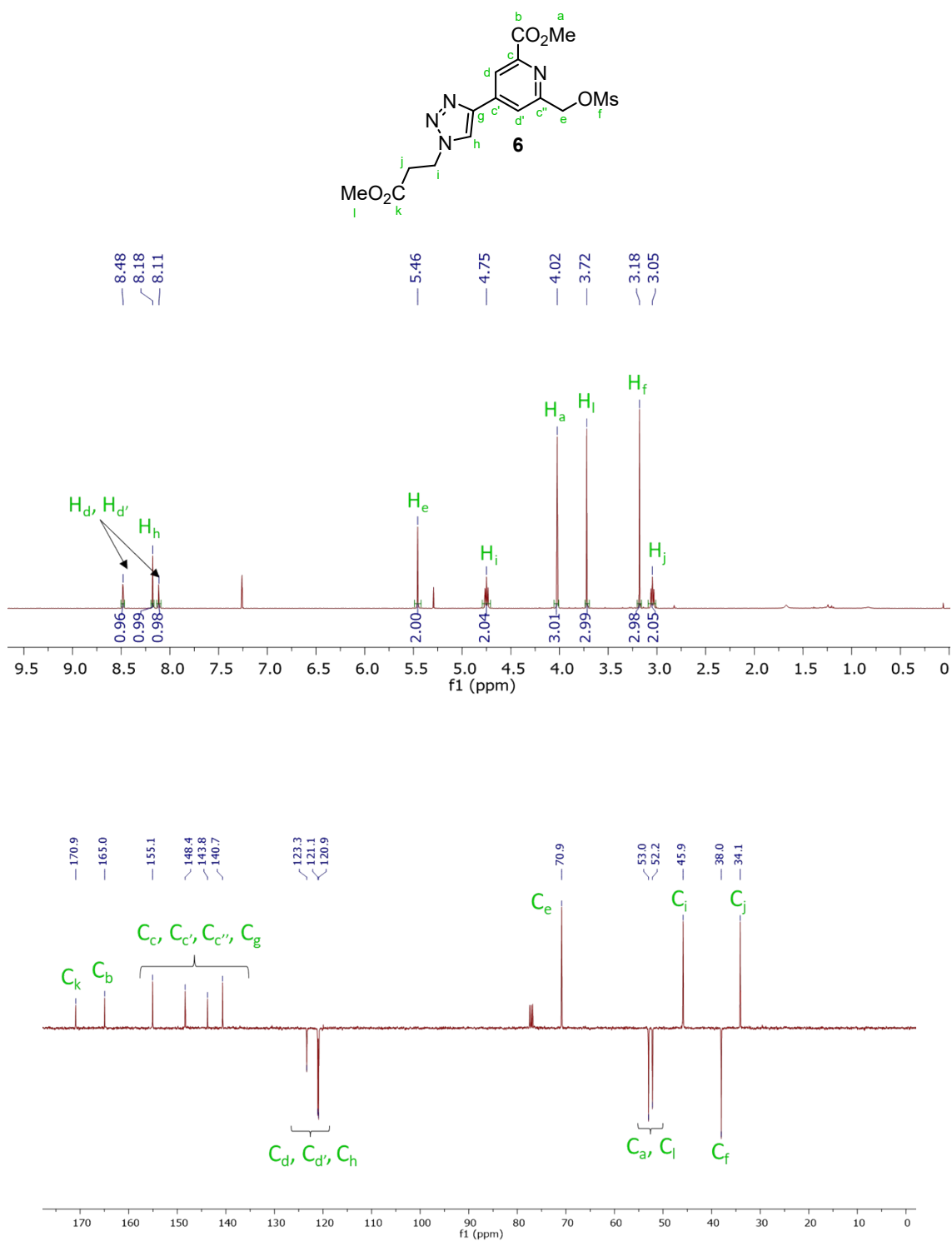


Figure S12. ¹H (400 MHz, CDCl₃, 25 °C) and ¹³C-Jmod (100 MHz, CDCl₃, 25 °C) NMR spectra of compound **6**.

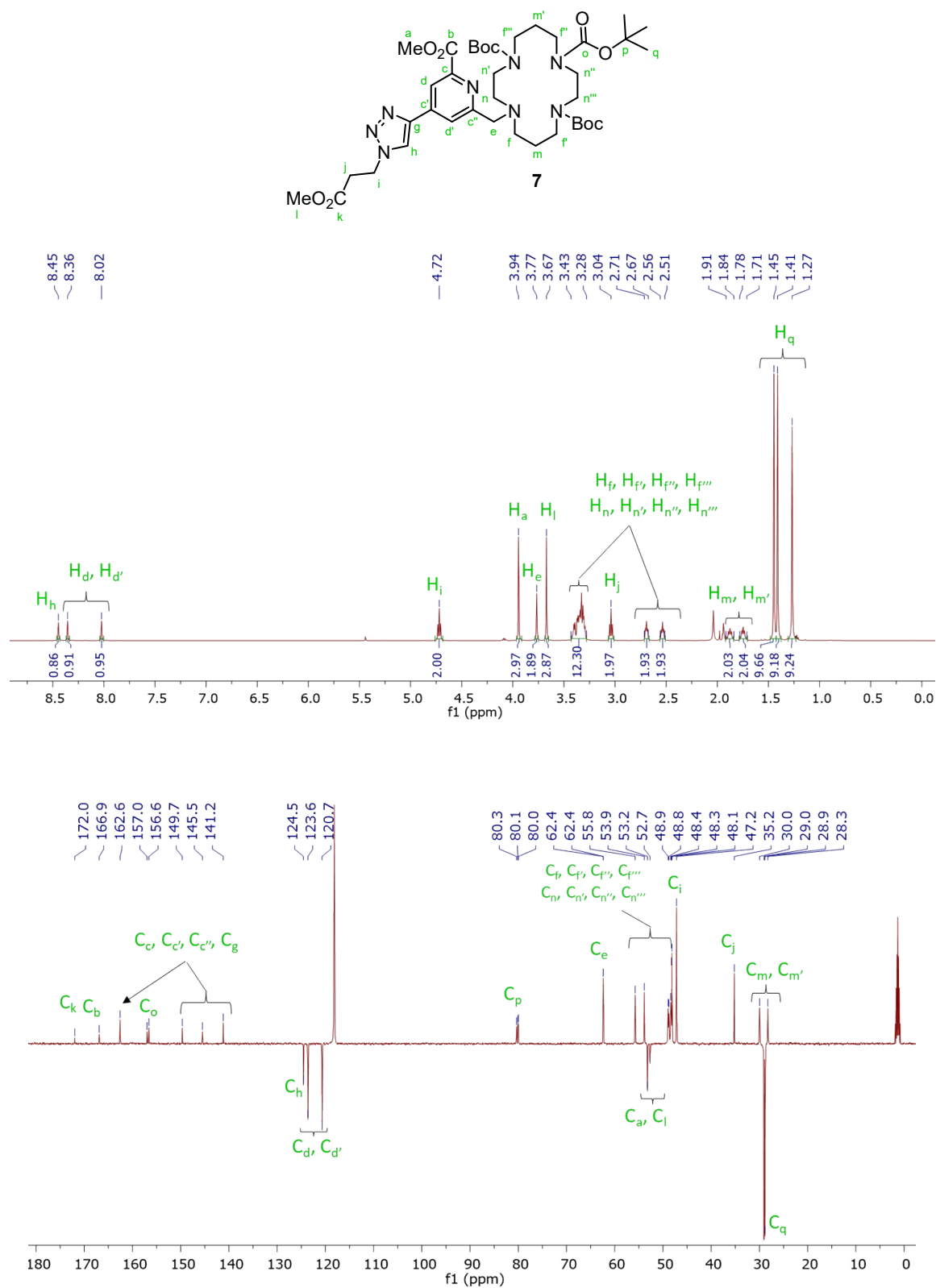
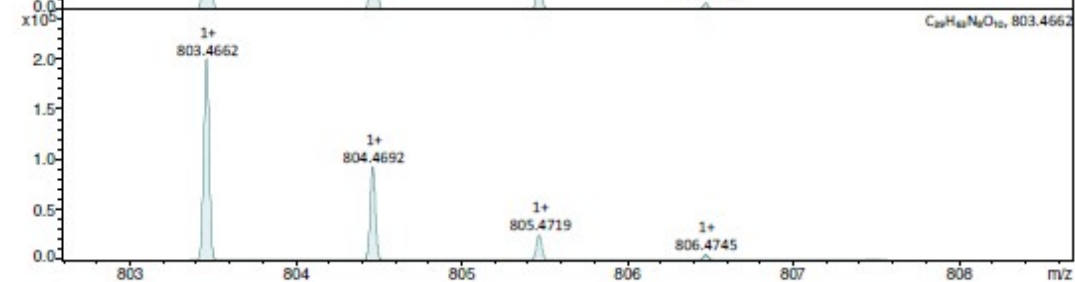
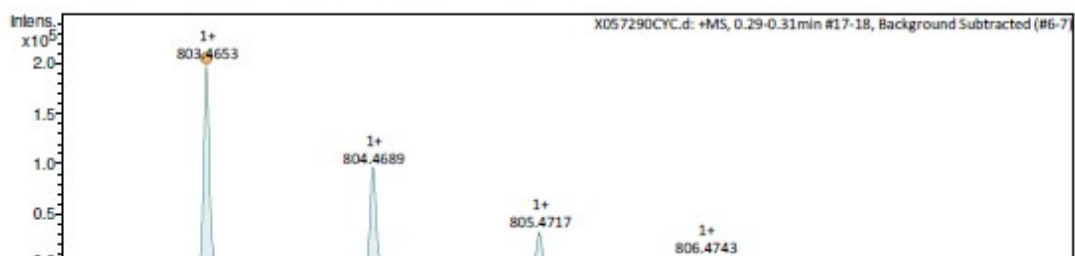
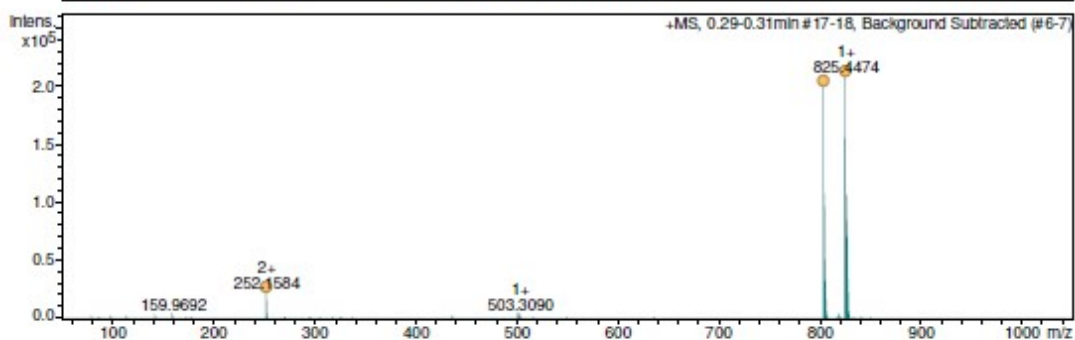


Figure S13. ¹H (500 MHz, CD₃CN 70 °C) and ¹³C-Jmod (125 MHz, CD₃CN, 70 °C) NMR spectra of compound **7**.

| | | | |
|----------------------|---------------|------------------|---------------------|
| Analysis Info | | Acquisition Date | 02/09/2020 11:01:11 |
| Sample Name | JP111_F10-F23 | Instrument/ Ser# | maXis 255552.00086 |
| Analysis Name | X057290CYC.d | Method | Positif.m |

| | | | | | |
|------------------------------|----------|-----------------------|------------|----------------|-----------|
| Acquisition Parameter | | | | | |
| Source Type | ESI | Ion Polarity | Positive | Set Nebulizer | 0.6 Bar |
| Scan Begin | 50 m/z | Set Capillary | 4500 V | Set Dry Heater | 200 °C |
| Scan End | 3000 m/z | Set Collision Cell RF | 1800.0 Vpp | Set Dry Gas | 7.0 l/min |



| Meas. m/z | z | # | Ion Formula | m/z | err [ppm] | mSigma | rdb | e ⁻ Conf |
|------------|----|---|---------------|------------|-----------|--------|------|---------------------|
| 252.158441 | 2+ | 1 | C24H40N8O4 | 252.158077 | -1.4 | 6.8 | 10.0 | even |
| 803.465263 | 1+ | 1 | C39H63N8O10 | 803.466167 | 1.1 | 23.2 | 13.0 | even |
| | 1+ | 2 | C51H59N6O3 | 803.464316 | -1.2 | 48.9 | 26.0 | even |
| 825.447363 | 1+ | 1 | C51H58N6NaO3 | 825.446260 | -1.3 | 33.3 | 26.0 | even |
| | 1+ | 2 | C39H62N8NaO10 | 825.448111 | 0.9 | 34.2 | 13.0 | even |

Figure S14. HRMS (ESI⁺) spectrum of compound 7.

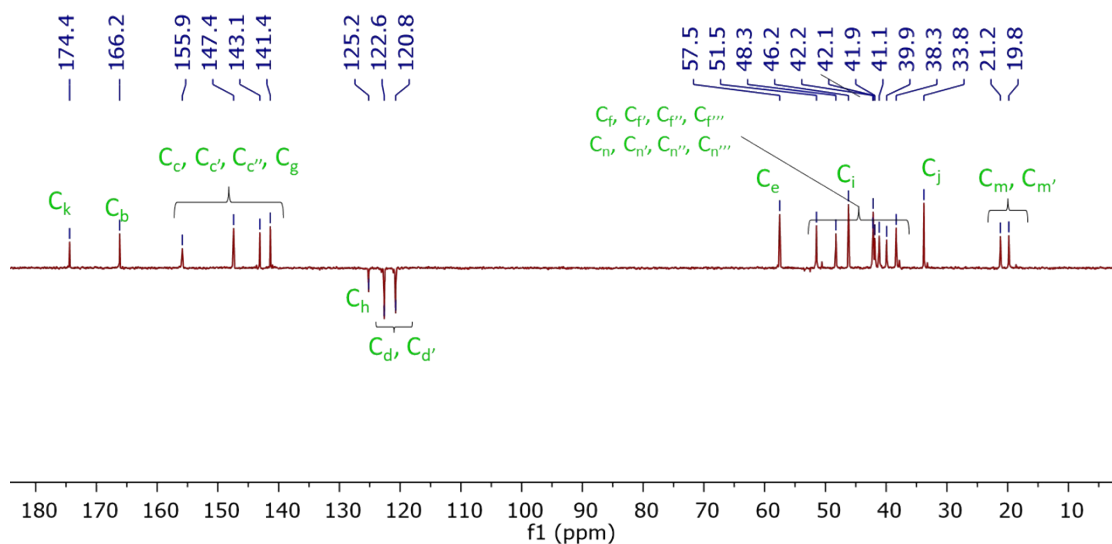
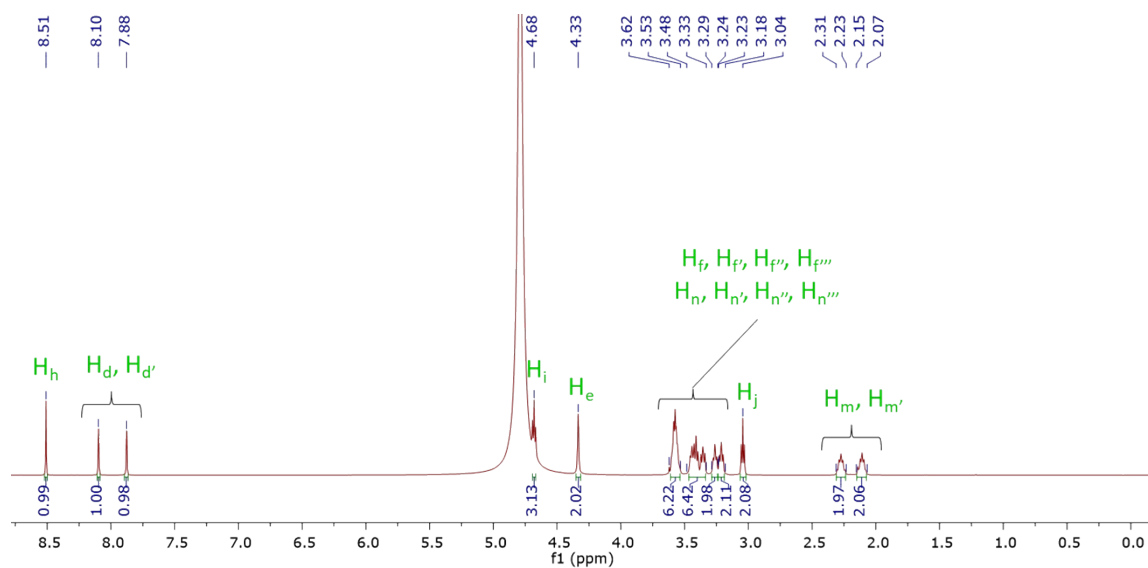
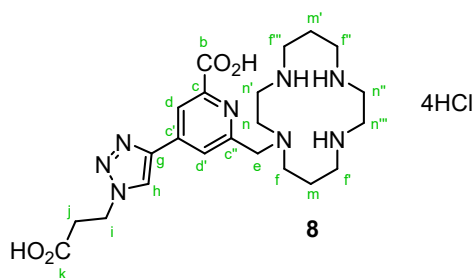


Figure S15. ¹H (500 MHz, D₂O, 25 °C) and ¹³C-Jmod (125 MHz, D₂O 25 °C) NMR spectra of H₂TE1PA-trz-prA.4HCl (compound **8**).

| Analysis Info | | Acquisition Date | | 02/09/2020 11:02:39 | |
|-----------------------|--------------|-----------------------|--------------------|---------------------|-----------|
| Sample Name | JP117 | Instrument / Ser# | maXis 255552.00086 | | |
| Analysis Name | X057291CYC.d | Method | Positif.m | | |
| Acquisition Parameter | | | | | |
| Source Type | ESI | Ion Polarity | Positive | Set Nebulizer | 0.6 Bar |
| Scan Begin | 50 m/z | Set Capillary | 4500 V | Set Dry Heater | 200 °C |
| Scan End | 3000 m/z | Set Collision Cell RF | 1800.0 Vpp | Set Dry Gas | 7.0 l/min |

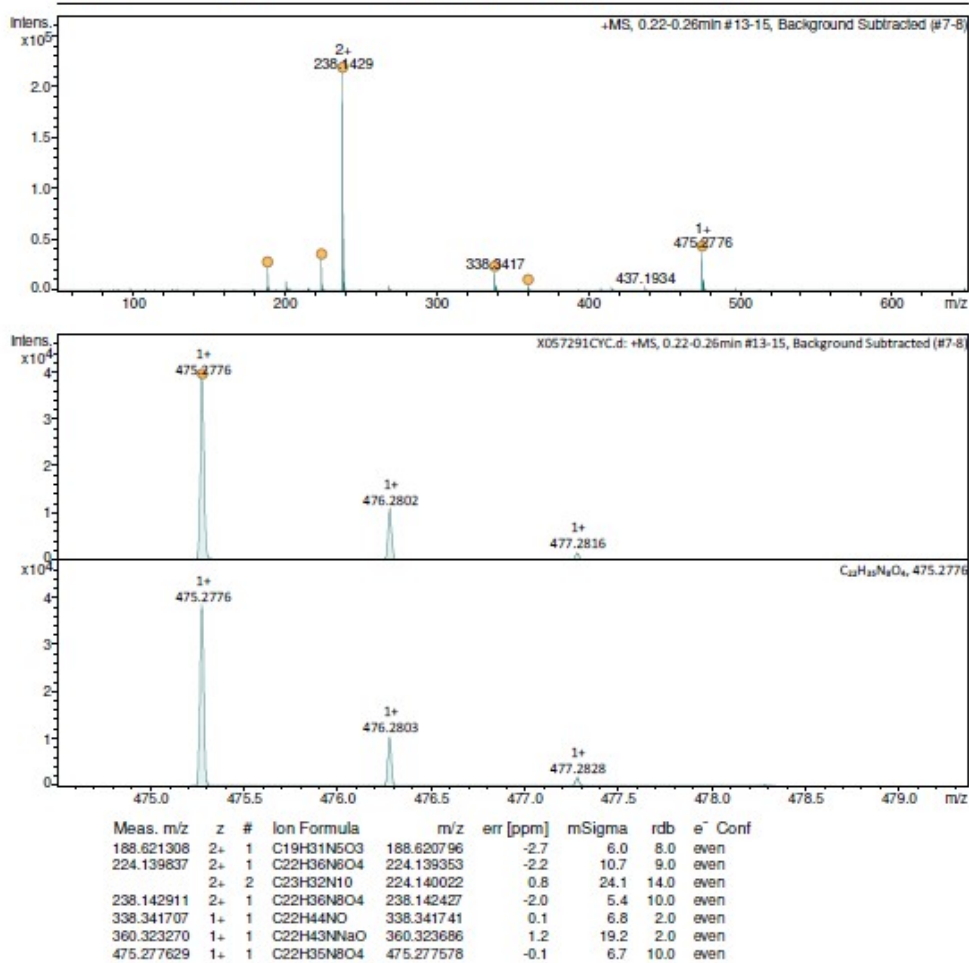


Figure S16. HRMS (ESI⁺) spectrum of ligand H₂TE1PA-trz-prA.4HCl (compound 8).

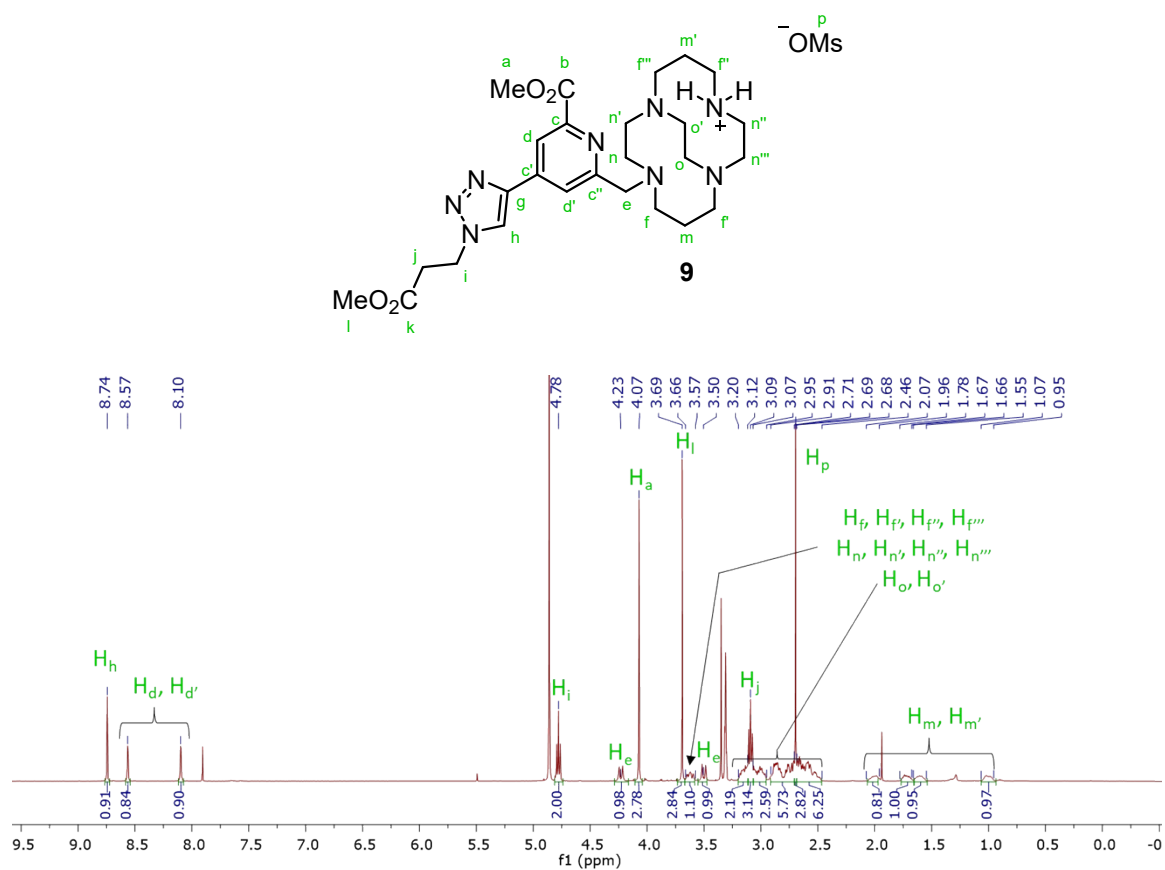


Figure S17. ^1H (400 MHz, CD_3OD , 25 °C) NMR spectrum of compound **9**.

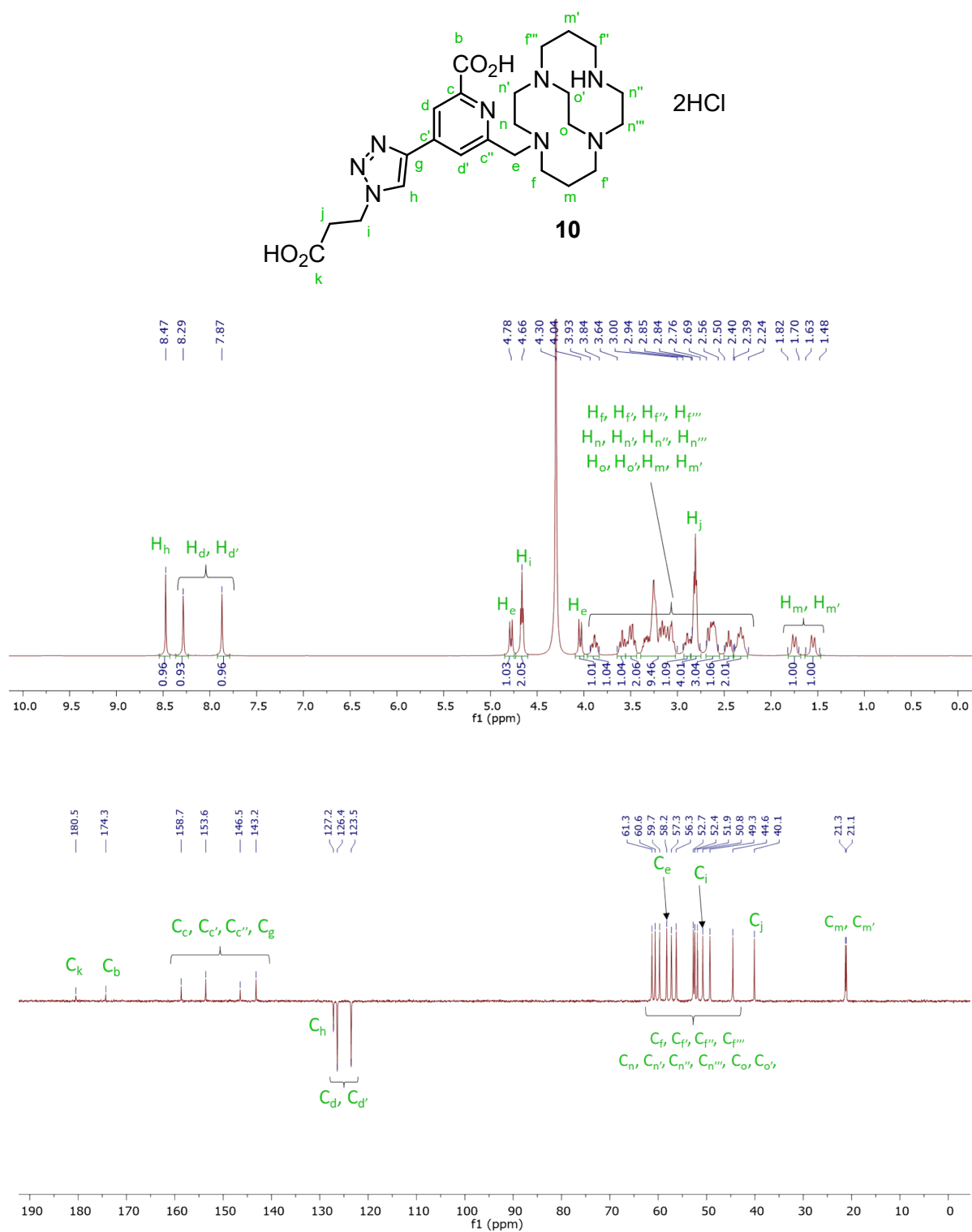


Figure S18: ¹H (500 MHz, D₂O, 70 °C) and ¹³C-Jmod (125 MHz, D₂O, 70 °C) NMR spectra of H₂CB-TE1PA-trz-prA.2HCl (compound **10**)

| Analysis Info | | Acquisition Date | | 10/02/2021 11:44:57 | |
|-----------------------|-------------------|-----------------------|--------------------|---------------------|-----------|
| Sample Name | JP194 Flash F9-10 | Instrument/ Ser# | maXis 255552.00086 | | |
| Analysis Name | X059172CYC.d | Method | Positif.m | | |
| Acquisition Parameter | | | | | |
| Source Type | ESI | Ion Polarity | Positive | Set Nebulizer | 0.6 Bar |
| Scan Begin | 50 m/z | Set Capillary | 4500 V | Set Dry Heater | 200 °C |
| Scan End | 3000 m/z | Set Collision Cell RF | 1800.0 Vpp | Set Dry Gas | 7.0 l/min |

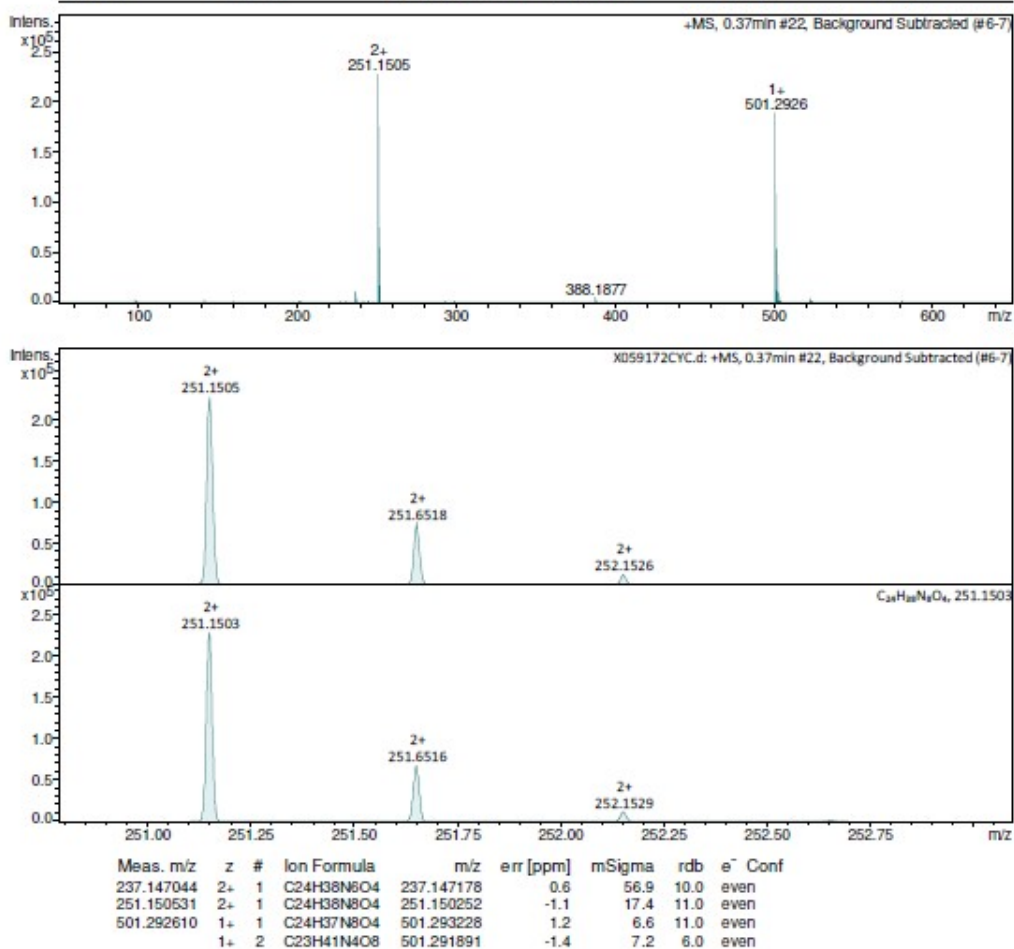
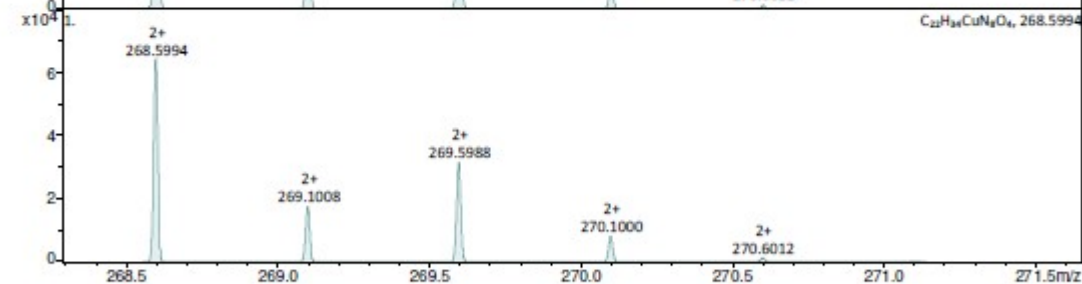
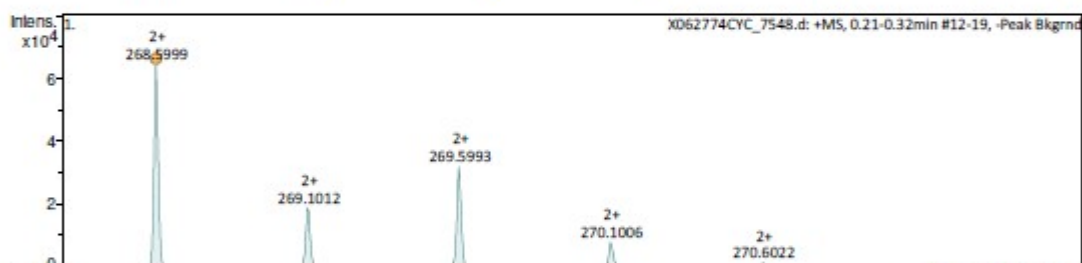
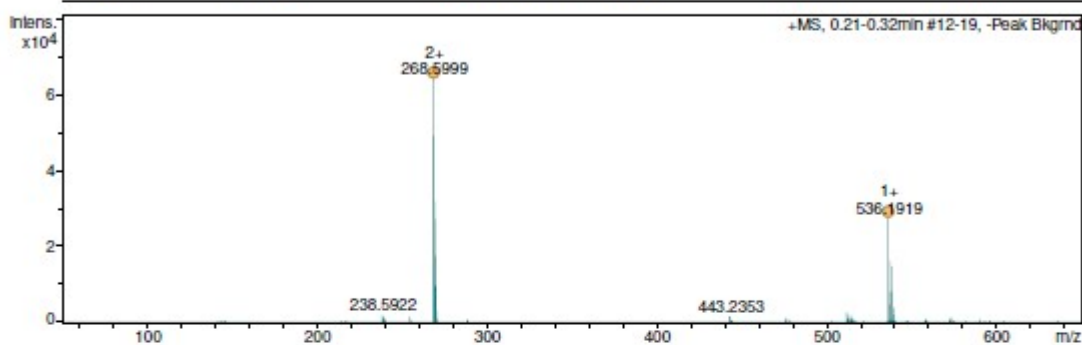


Figure S19: HRMS (ESI⁺) spectrum of ligand H₂CB-TE1PA-trz-prA.2HCl (compound 10).

| | | | |
|----------------------|-------------------|------------------|---------------------|
| Analysis Info | | Acquisition Date | 13/10/2021 19:13:41 |
| Sample Name | JP272 | Instrument/ Ser# | maXis 255552.00086 |
| Analysis Name | X062774CYC_7548.d | Method | Positif.m |

| | | | | | |
|------------------------------|----------|-----------------------|------------|----------------|-----------|
| Acquisition Parameter | | | | | |
| Source Type | ESI | Ion Polarity | Positive | Set Nebulizer | 0.6 Bar |
| Scan Begin | 50 m/z | Set Capillary | 4500 V | Set Dry Heater | 200 °C |
| Scan End | 3000 m/z | Set Collision Cell RF | 1800.0 Vpp | Set Dry Gas | 7.0 l/min |



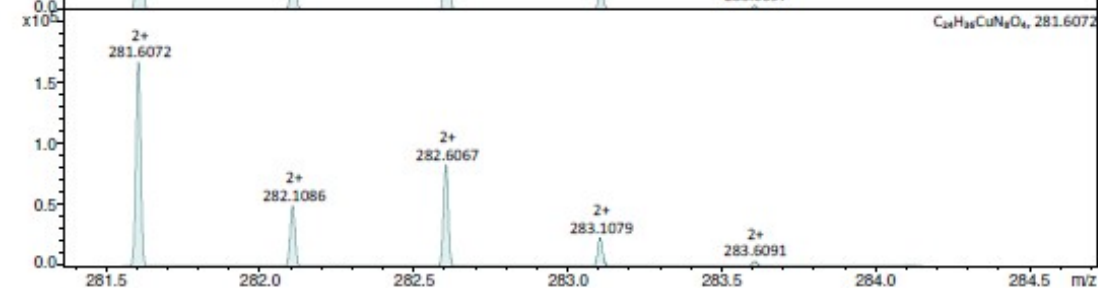
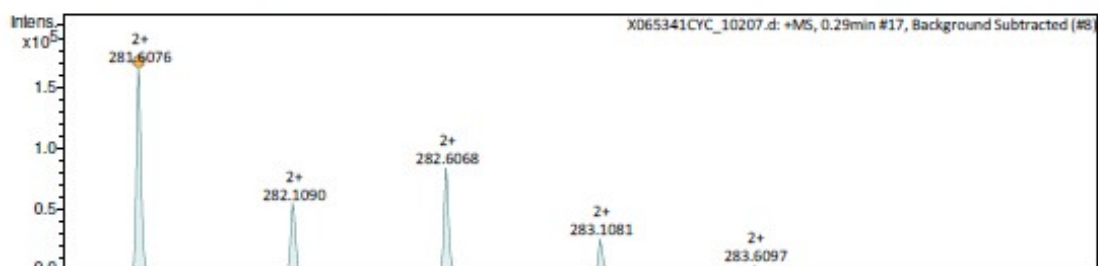
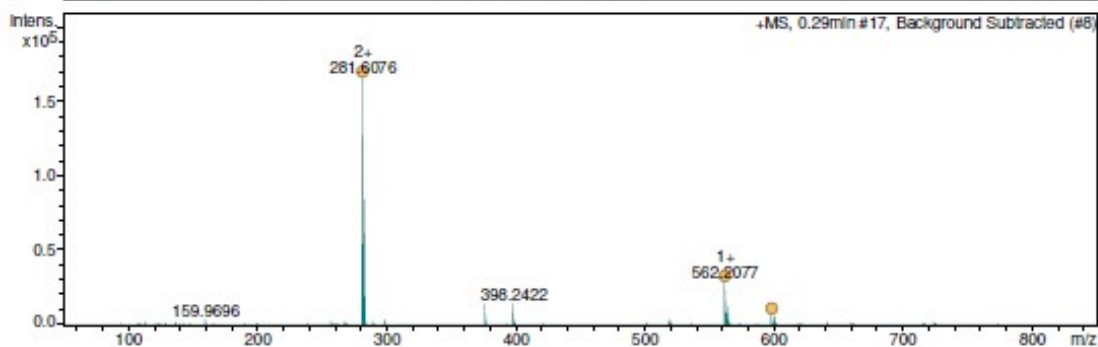
| Meas. m/z | z | # | Ion Formula | m/z | err [ppm] | mSigma | rdB | e ⁻ | Conf |
|------------|----|---|---|------------|-----------|--------|------|----------------|------|
| 268.599937 | 2+ | 1 | C ₂₂ H ₃₄ CuN ₈ O ₄ | 268.599401 | -2.0 | 10.2 | 10.5 | odd | |
| 536.191937 | 1+ | 1 | C ₂₂ H ₃₃ CuN ₈ O ₄ | 536.191525 | -0.8 | 27.4 | 10.5 | odd | |

Figure S20: HRMS (ESI⁺) spectrum of complex [Cu(TE1PA-trz-prA)] (11)

| | | | |
|----------------------|--------------------|------------------|---------------------|
| Analysis Info | | Acquisition Date | 16/02/2022 18:39:06 |
| Sample Name | JP288 | Instrument/ Ser# | maXis 255552.00086 |
| Analysis Name | X065341CYC_10207.d | Method | Positif.m |

Acquisition Parameter

| | | | | | |
|-------------|----------|-----------------------|------------|----------------|-----------|
| Source Type | ESI | Ion Polarity | Positive | Set Nebulizer | 0.6 Bar |
| Scan Begin | 50 m/z | Set Capillary | 4500 V | Set Dry Heater | 200 °C |
| Scan End | 3000 m/z | Set Collision Cell RF | 1800.0 Vpp | Set Dry Gas | 7.0 l/min |



| Meas. m/z | z | # | Ion Formula | m/z | err [ppm] | mSigma | rdb | e ⁻ | Conf |
|------------|----|---|----------------|------------|-----------|--------|------|----------------|------|
| 281.607613 | 2+ | 1 | C24H36CuN8O4 | 281.607226 | -1.4 | 18.5 | 11.5 | odd | |
| 562.207674 | 1+ | 1 | C24H35CuN8O4 | 562.207176 | -0.9 | 36.8 | 11.5 | odd | |
| 598.184112 | 1+ | 1 | C24H36ClCuN8O4 | 598.183853 | -0.4 | 128.9 | 10.5 | odd | |

Figure S21: HRMS (ESI⁺) spectrum of complex [Cu(CB-TE1PA-trz-prA)] (12).

Thermodynamic equilibrium studies

Potentiometric titrations were performed in aqueous solution at 25.0 °C and 0.10 M KNO₃, using the potentiometric setup and methods previously described.^{7a,b} In particular, the setup consisted of a glass-jacketed titration cell and a separate reference cell connected by a Wilhelm-type salt bridge filled with 0.1 M KNO₃ electrolyte, using a Metrohm 665 Dosimat buret and an Orion 720A+ potentiometer fitted with a Metrohm 6.0150.100 glass electrode and a Metrohm 6.0733.100 reference electrode. Temperature in the titration cells was controlled using a Huber CC3-K6 cooling circulation thermostatic bath and a previously calibrated Orion 91-70-06 ATC-probe, and atmospheric CO₂ was excluded from the titration cell during experiments by passing purified nitrogen across the top of the titration solution. The titrant was a KOH solution prepared at about 0.1 M from a commercial ampule of analytical grade, and its accurate concentration was obtained by titration of a standard HNO₃ solution also prepared from a commercial ampule by application of the Gran method. A solution of 0.1 M HNO₃ was used as titrant in back-titrations. Ligand solutions were prepared at 1.5–2×10⁻³ M, and a Cu²⁺ solution was prepared at 0.050 M from analytical grade nitrate salt and standardized by complexometric titration with K₂H₂EDTA (ethylenediaminetetraacetic acid, dipotassium salt). The electromotive force of the sample solutions was measured after calibration of the electrode by titration of a standard HNO₃ solution at 2×10⁻³ M. The [H⁺] of the solutions was determined by measurement of the electromotive force of the cell, $E = E' + Q \log [H^+] + E_j$. The term pH is defined as $-\log [H^+]$. The values of E' and Q were determined by titrating a solution of known [H⁺] concentration at the same ionic strength. The liquid junction potential, E_j , was found to be negligible under the experimental conditions used. The protonation constants of H₄edta and the thermodynamic stability constants of its copper(II) complex used in competition titration refinements were taken from the literature.⁸ Titrations were run containing *ca.* 0.035 mmol of ligand in a volume of 30 mL where the ionic strength was kept at 0.10 M using KNO₃ as background electrolyte, and copper(II) nitrate was added at 0.9 equiv. in complexation titrations. Each titration consisted of 120–150 equilibrium points in the range of pH 2.0–11.5, and at least two replicate titrations were performed for each particular system. The $\log \beta_{CuL}$ for the copper(II) complex of H₂TE1PA-trz-prA was determined in a competition titration including 1 equiv. of copper(II) and 1 equiv. of K₂H₂EDTA, and the obtained value was then used as a fixed constant in the refinement of the remaining complexation constants on a normal complexation titration. All titrations were run in-cell and attained equilibrium quickly, without the need for any out-of-cell measurements. Only mononuclear complex species could be found in the experimental conditions used.

Potentiometric data was fitted using the Hyperquad 2008 software⁹ and plotted with the Hyss software.¹⁰ The overall equilibrium constants β_i^H and $\beta_{M_m H_h L_l}$ were determined in log units from fitting of the potentiometric titrations as defined by $\beta_i^H = [H_h L_l] / [H]^h [L]^l$ and $\beta_{M_m H_h L_l} = [M_m H_h L_l] / [M]^m [H]^h [L]^l$. Stepwise constants are defined by $K_{M_m H_h L_l} = [M_m H_h L_l] / [M_m H_{h-1} L_l] [H]$

and are calculated from the difference in log units between overall constants of sequentially protonated species. The errors quoted are the standard deviations calculated by the fitting program for the experimental data in each system. The value of $K_w = [H^+][OH^-]$ was taken from the literature¹¹ as equal to $10^{-13.778}$.

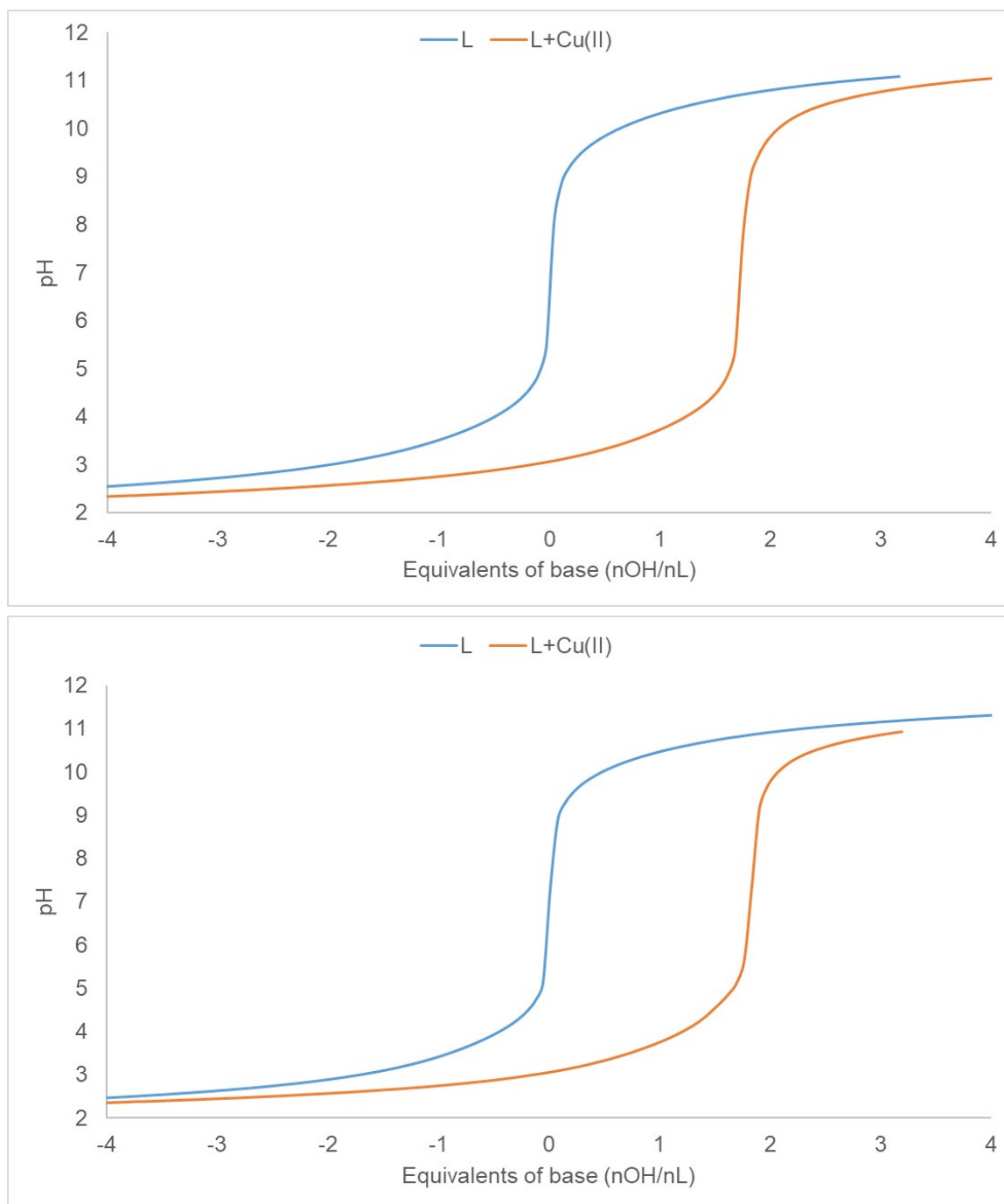


Figure S22. Titration curves of H₂TE1PA-trz-prA (top) and H₂CB-TE1PA-trz-prA (bottom) in the absence and in presence of 0.9 equiv. of copper(II), plotted in pH versus the number of equivalents of base added to a fully neutral ligand (L).

Table S1. Stepwise protonation constants ($\log K_i^H$) of ligands **TE1PA-trz-prA²⁻** and **CB-TE1PA-trz-prA²⁻** determined at 25 °C with $I = 0.10$ M KNO₃, compared to the parent ligands **TE1PA⁻** and **CB-TE1PA⁻**.

| Equilibrium reaction ^a | TE1PA ^{-b} | TE1PA-trz-prA ²⁻ | CB-TE1PA ^{-c} | CB-TE1PA-trz-prA ²⁻ |
|--|---------------------|-----------------------------|------------------------|--------------------------------|
| L + H ⁺ ⇌ HL | 11.55(1) | 11.52(1) | – ^d | – ^d |
| HL + H ⁺ ⇌ H ₂ L | 10.11(1) | 10.11(1) | 10.13(5) | 10.28(1) |
| H ₂ L + H ⁺ ⇌ H ₃ L | 2.71(1) | 3.87(1) | 2.43 | 3.65(1) |
| H ₃ L + H ⁺ ⇌ H ₄ L | 1.7(1) | 2.47(1) | < 2.0 | 1.76(2) |
| H ₄ L + H ⁺ ⇌ H ₅ L | – | 2.13(2) | – | – |

^a L denotes the ligand in general; charges are omitted for clarity. ^b From ref. 7a. ^c From ref. 7b. ^d This protonation constant could not be experimentally determined. The protonation equilibria corresponding to the pyridyl carboxyl group are highlighted in green. The additional protonation equilibria corresponding to the supplementary carboxylic functions are highlighted in red.

The acid-base properties of both ligands were determined in 0.10 M KNO₃ aqueous solution at 25.0 °C (Table S1). The protonation constants for **TE1PA-trz-prA²⁻** and **CB-TE1PA-trz-prA²⁻** are very similar to those reported for the corresponding parent ligands, **TE1PA⁻** and **CB-TE1PA⁻**. The main difference is, for each ligand, one additional protonation constant in the acidic pH range, $\log K = 3.87$ and 3.65 , respectively (Table S1). These values are significantly higher than those assigned to the pyridyl carboxyl group of **TE1PA⁻** and **CB-TE1PA⁻** ($\log K = 2.71$ and 2.43 , respectively) and are attributed to the carboxyl group of the propionate chain. **CB-TE1PA-trz-prA²⁻** displays the proton-sponge behaviour previously observed for **CB-TE1PA⁻** which precludes the determination of the highest protonation constant by potentiometric titration.

Table S2. Overall (β_{MHIL}) and stepwise ($\log K_{\text{MHIL}}$) stability constants, and calculated pCu values for the Cu(II) complexes formed with **TE1PA-trz-prA²⁻** and **CB-TE1PA-trz-prA²⁻** determined at 25 °C with $I = 0.10$ M KNO₃, compared to the parent ligands **TE1PA⁻** and **CB-TE1PA⁻**.

| Equilibrium reaction ^a | TE1PA ^{-b} | TE1PA-trz-prA ²⁻ | CB-TE1PA ^{-c} | CB-TE1PA-trz-prA ²⁻ |
|---|---------------------|-----------------------------|------------------------|--------------------------------|
| $\log \beta_{\text{MHIL}}$ | | | | |
| $\text{Cu}^{2+} + \text{L} \rightleftharpoons \text{CuL}$ | 25.5(1) | 25.4(1) | ^{-d} | ^{-d} |
| $\text{Cu}^{2+} + \text{HL} \rightleftharpoons \text{CuL} + \text{H}^+$ | - | - | 11.00(5) | 9.6(3) |
| $\text{Cu}^{2+} + \text{L} + \text{H}^+ \rightleftharpoons \text{CuHL}$ | 27.68(1) | 29.16(2) | - | - |
| $\text{Cu}^{2+} + \text{HL} \rightleftharpoons \text{CuHL}$ | - | - | - | 13.19(2) |
| $\text{Cu}^{2+} + \text{L} + 2\text{H}^+ \rightleftharpoons \text{CuH}_2\text{L}$ | - | 31.33(2) | - | - |
| $\text{Cu}^{2+} + \text{L} \rightleftharpoons \text{CuHL}_{-1} + \text{H}^+$ | 14.35(2) | 13.69(2) | - | - |
| $\text{Cu}^{2+} + \text{HL} \rightleftharpoons \text{CuHL}_{-1} + 2\text{H}^+$ | - | - | 0.95(9) | -1.72(7) |
| $\log K_{\text{MHIL}}$ | | | | |
| $\text{Cu}^{2+} + \text{L} \rightleftharpoons \text{CuL}$ | 25.5(1) | 25.4(1) | ^{-d} | ^{-d} |
| $\text{CuL} + \text{H}^+ \rightleftharpoons \text{CuHL}$ | 2.17(1) | 3.78(2) | - | 3.59(4) |
| $\text{CuHL} + \text{H}^+ \rightleftharpoons \text{CuH}_2\text{L}$ | - | 2.17(1) | - | - |
| $\text{CuL}(\text{OH}) + \text{H}^+ \rightleftharpoons \text{CuL}$ | 11.15(1) | 11.69(2) | 10.05 | 11.32(6) |
| pCu ^e | 18.64 | 18.55 | 15.67 | 14.12 |

^a Charges are omitted for clarity; L denotes the ligand in general. ^b From ref. 7a. ^c From ref. 7b. ^d This constant could not be determined experimentally. ^e Calculated at pH = 7.4 for 100% excess of ligand with $[\text{Cu}^{2+}]_{\text{tot}} = 1 \times 10^{-5}$ M. Values in parentheses are standard deviation in the last significant figure.

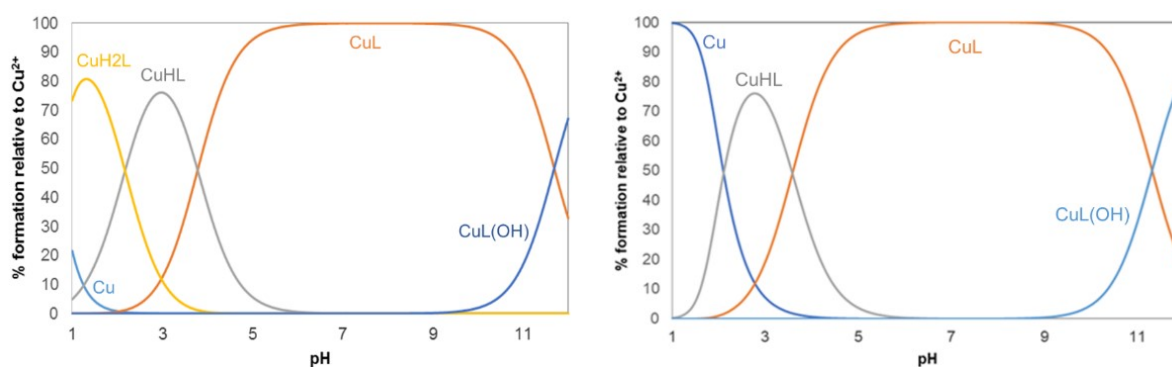


Figure S23. Species distribution diagrams of Cu(II) in presence of **TE1PA-trz-prA²⁻** (left), and **CB-TE1PA-trz-prA²⁻** (right) calculated at $[\text{Cu}^{2+}]_{\text{tot}} = [\text{L}]_{\text{tot}} = 1 \times 10^{-3}$ M.

X-ray Diffraction Determination of [Cu(CB-TE1PA-trz-prA)] (12)

X-ray diffraction was determined at the University of Rennes. A suitable crystal for X-ray diffraction single crystal experiment (blue prism, dimensions = 0.640 x 0.380 x 0.200 mm) was selected and mounted on the goniometer head of a D8 Venture (Bruker-AXS) diffractometer equipped with a CMOS-PHOTON70 detector, using Mo-K α radiation ($\lambda = 0.71073$ Å, graphite monochromator) at $T = 150(2)$ K. Crystal structure has been described in monoclinic symmetry and P 21/n (I.T.#14) centric space group. Cell parameters have been refined as follows: $a = 16.6398(8)$ Å, $b = 22.4361(9)$ Å, $c = 30.5104(15)$ Å, $\beta = 97.393(2)$ °, $V = 11295.8(9)$ Å³. Number of formula unit Z is equal to 4 and calculated density d and absorption coefficient μ values are 1.523 g.cm⁻³ and 0.839 mm⁻¹ respectively. Crystal structure was solved by dual-space algorithm using SHELXT program,¹² and then refined with full-matrix least-squares methods based on F2 (SHELXL¹³). All non-Hydrogen atoms were refined with anisotropic atomic displacement parameters. Except H3N, H11N, H19N, H28N and the hydrogens of the water molecules which were introduced in the structural model through Fourier difference maps analysis, H atoms were finally included in their calculated positions and treated as riding on their parent atom with constrained thermal parameters. A final refinement on F2 with 25753 unique intensities and 1630 parameters converged at ω RF2 = 0.1106 (RF = 0.0442) for 20336 observed reflections with $I > 2\sigma(I)$. CCDC 2205613 contain the supplementary crystallographic data for this paper. These data can be obtained free of charge from The Cambridge Crystallographic Data Centre via www.ccdc.cam.ac.uk/data_request/cif.

Single crystals of the complex of H₂CB-TE1PA-trz-prA with Cu²⁺ were obtained by slow evaporation of a concentrated CH₃CN/ethanol solution of the complex at room temperature (Table S3). The crystals structure analysis reveals that the crystalline structure is composed of four complex units of [Cu(CB-TE1PA-trz-prA)] slightly different and water molecules. A view of the structure of one complex cation is shown in Figure 2, while bond distances and angles of the metal coordination environment of the four species are given in Table S4. The metal ion in [Cu(CB-TE1PA-trz-prA)] is five coordinated, being directly bound to the four nitrogen atoms of the macrocyclic unit and the nitrogen atom of the pyridyl group. The distance between the metal atom and the oxygen atom of the carboxylic group O(1) [317 Å vs 3.16 Å for CB-TE1PA] is here again too long to be considered as a bond distance. The coordination polyhedron around the copper center can be defined as a trigonal bipyramid, in which the equatorial plane is defined by the N atoms of the cyclam fragment N2 and N4, the nitrogen atom of the pyridyl unit N5 and the metal ion, and the apical positions are defined by donor atoms N1 and N3. Alternatively, the coordination polyhedron may be defined as square pyramidal, where the basal plane is formed by N1, N2, N3 and N5, and the apical position is defined by N4. The index of trigonality τ is calculated to be 0.52 (average τ value of the four species) (vs 0.53 for CB-TE1PA), which points to a distorted coordination polyhedron that is

halfway between the two ideal geometries ($\tau = 0$ for a perfect square pyramidal geometry and $\tau = 1$ for an ideal trigonal-bipyramidal geometry).¹⁴ The CB-cyclam unit presents a *cis*-V folded coordination configuration¹⁵ that provides four convergent nitrogen donor atoms for Cu²⁺ coordination. The bicyclo[6.6.2] ligand backbone shows a [2323]/[2323] conformation,¹⁶ as often observed in structures of Cu²⁺ complexes of cross-bridged cyclam derivatives.

An intramolecular hydrogen bonding interaction exists between the NH group of the macrocyclic fragment and one of the oxygen atoms of the carboxylate function (N(3)···O(1) 2.851(2) Å vs 2.808(7) Å for **CB-TE1PA**, N(3)-H(3)···O(1) 2.23 vs 2.16 Å, N(3)-H(3)···O(1) 133.69 vs 126.0°, which results in the formation of a macrotricyclic-like structure due to the formation of a third pseudomacrocyclic cycle.

In [Cu(**CB-TE1PA-trz-prA**)] as for [Cu(**CB-TE1PA**)]⁺ the donor atom of the macrocyclic fragment N3 provides the strongest interaction with the copper center, with bond distance of 1.99 Å vs 1.97 Å for **CB-TE1PA**, the other Cu–N distances in the range 2.01–2.14 Å as for its analogue. These bond distances being shorter than those observed for [Cu(**TE1PA**)]⁺ (2.00–2.35 Å) related five-coordinated copper(II) complexes with cyclam-based ligand lacking the cross-bridged unit,^{7b} which points to a particularly strong interaction of the **CB-TE1PA**⁻ ligand with Cu²⁺.

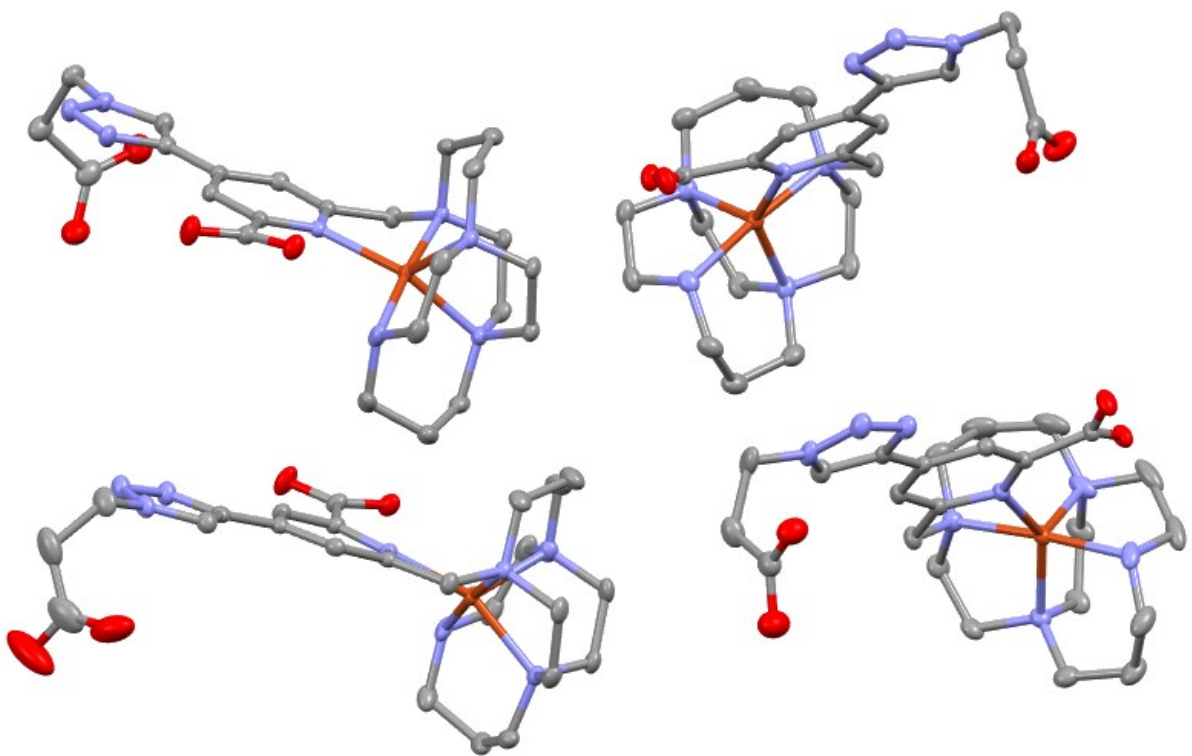


Figure S24. View of the crystal structures of the four complexes of [Cu(CB-TE1PA-trz-prA)] (12) present in the crystalline structure. Hydrogen atoms are omitted for clarity.

Table S3. Crystallographic data of [Cu(CB-TE1PA-trz-prA)] (12)

| | |
|------------------------------------|---|
| Empirical formula | C ₉₆ H ₁₇₄ Cu ₄ N ₃₂ O ₃₅ |
| Formula weight | 2590.82 |
| Temperature | 150(2) K |
| Radiation type | Mo-Kalpha |
| Wavelength | 0.71073 Å |
| Crystal system | Monoclinic |
| Space group | P21/n |
| Unit cell dimensions | a = 16.6398(8) Å α = 90° b = 22.4361(9) Å β = 97.393(2)° c = 30.5104(15) Å γ = 90° |
| Volume | 11295.8(9) Å ³ |
| Z | 4 |
| Density (calculated) | 1.523 g/cm ³ |
| Absorption coefficient | 0.839 mm ⁻¹ |
| F(000) | 5480 |
| Crystal size | 0.640 x 0.380 x 0.200 mm |
| Crystal color | blue |
| Crystal description | prism |
| Diffractometer | D8 Venture (Bruker-AXS) |
| Detector | CMOS-PHOTON70 |
| θ range for data collection | 1.736 to 27.485° |
| Index ranges | -21 ≤ h ≤ 19, -29 ≤ k ≤ 27, -39 ≤ l ≤ 39 |
| Reflections collected / unique | 85151 / 25753 [R(int) = 0.0458] |
| Reflections [I > 2σ(I)] | 20336 |
| Completeness to θ max | 0.994 |
| Absorption correction type | Multi-scan |
| Max. and min. transmission | 0.846 and 0.718 |
| Refinement method | Full-matrix least-squares on F ² |
| H-atom treatment | H-atom parameters treated by a mixture of independent and constrained refinement |
| Data/restraints/parameters | 25753 / 43 / 1630 |
| Goodness-of-fit | 1.015 |
| Shelxl weighting scheme parameters | a = 0.0478, b = 16.240 |
| Final R indices [I > 2σ(I)] | R1 = 0.0442, wR2 = 0.1106 |
| R indices (all data) | R1 = 0.0613, wR2 = 0.1216 |
| Extinction coefficient | n.a. |
| Largest diff. peak and hole | 2.225 and -0.870 e ⁻ Å ⁻³ |

Table S4. Selected bond lengths (Å) and angles (°) of the metal coordination environments in [Cu(CB-TE1PA-trz-prA)] (four complexes) compared with [Cu(CB-TE1PA)]⁺.^{7b} See Figure 2 for labeling.

| | [Cu(CB-TE1PA-trz-prA)] | | | | | [Cu(CB-TE1PA)] ⁺ |
|-----------------|------------------------|------------------|------------------|------------------|----------------------|-----------------------------|
| | <i>Complex 1</i> | <i>Complex 2</i> | <i>Complex 3</i> | <i>Complex 4</i> | <i>Average value</i> | |
| Cu(1)–N(1) | 2.018(2) | 2.014(2) | 2.022(2) | 2.006(2) | 2.015(2) | 2.010(6) |
| Cu(1)–N(2) | 2.146(2) | 2.132(2) | 2.137(2) | 2.116(2) | 2.132(2) | 2.138(6) |
| Cu(1)–N(3) | 1.997(2) | 1.988(2) | 2.000(2) | 1.992(2) | 1.994(2) | 1.966(6) |
| Cu(1)–N(4) | 2.121(2) | 2.115(2) | 2.106(2) | 2.128(2) | 2.118(2) | 2.108(6) |
| Cu(1)–N(5) | 2.134(2) | 2.134(2) | 2.124(2) | 2.152(2) | 2.136(2) | 2.113(6) |
| N(1)–Cu(1)–N(3) | 175.02(9) | 175.03(9) | 174.31(9) | 175.12(9) | 174.87(9) | 175.4(3) |
| N(3)–Cu(1)–N(4) | 87.05(9) | 87.34(10) | 86.31(9) | 86.03(9) | 86.683(10) | 87.4(2) |
| N(1)–Cu(1)–N(4) | 93.64(8) | 92.74(9) | 93.47(8) | 93.07(8) | 93.23(9) | 94.1(2) |
| N(3)–Cu(1)–N(5) | 103.63(8) | 103.12(8) | 103.56(8) | 103.26(8) | 103.39(8) | 102.1(2) |
| N(1)–Cu(1)–N(5) | 79.98(8) | 80.83(8) | 81.06(8) | 81.14(8) | 80.76(8) | 80.4(2) |
| N(4)–Cu(1)–N(5) | 127.04(8) | 126.20(8) | 127.92(8) | 126.39(8) | 126.89(8) | 127.7(2) |
| N(3)–Cu(1)–N(2) | 90.03(8) | 90.49(9) | 89.72(9) | 90.18(9) | 90.11(9) | 90.7(2) |
| N(1)–Cu(1)–N(2) | 85.11(8) | 84.55(8) | 84.59(8) | 84.99(8) | 84.81(8) | 85.1(2) |
| N(4)–Cu(1)–N(2) | 85.65(8) | 86.78(8) | 87.38(8) | 87.55(8) | 86.84(8) | 86.2(2) |
| N(5)–Cu(1)–N(2) | 144.54(8) | 144.24(8) | 142.37(8) | 143.71(8) | 143.72(8) | 143.7(2) |

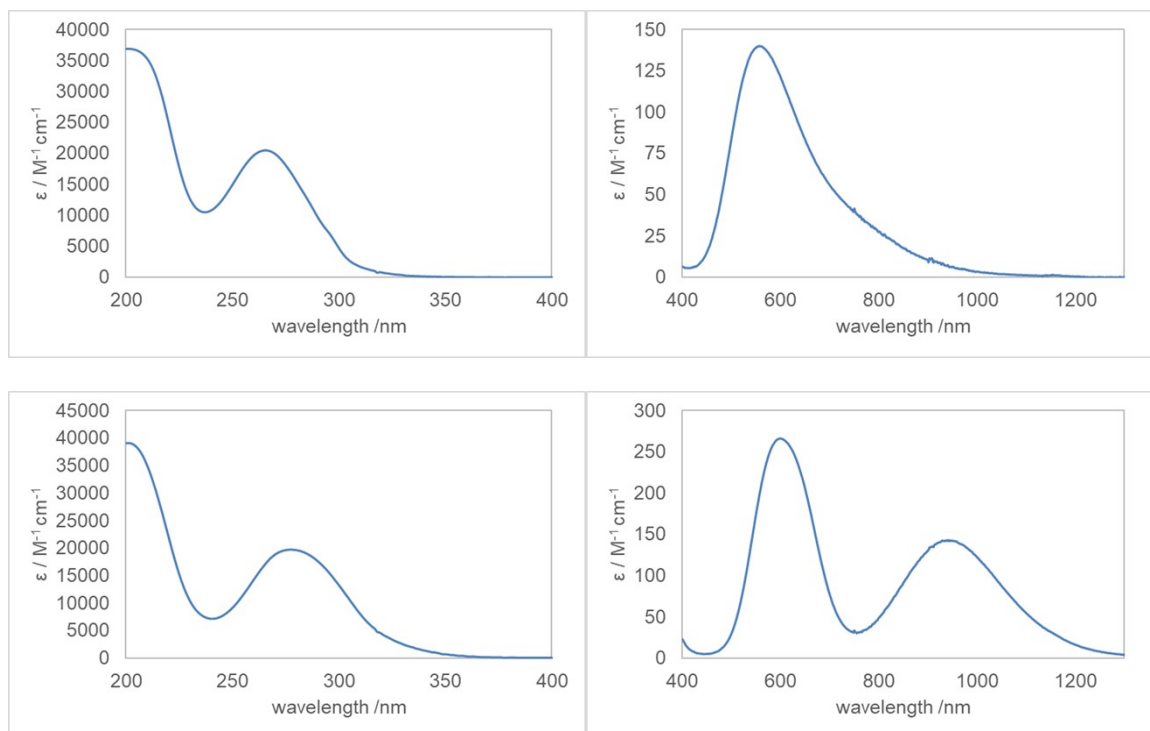


Figure S25. UV and vis-NIR absorption spectra of the complexes [Cu(TE1PA-trz-prA)] (top) and [Cu(CB-TE1PA-trz-prA)] (bottom) in aqueous solutions at neutral pH.

Table S5. UV-vis-NIR absorption parameters for the [Cu(TE1PA-trz-prA)] and [Cu(CB-TE1PA-trz-prA)] complexes compared to the parent complexes [Cu(TE1PA)]⁺ and [Cu(CB-TE1PA)]⁺.

| | λ_{\max} /nm (ϵ /M ⁻¹ cm ⁻¹) |
|--|---|
| [Cu(TE1PA-trz-prA)] | 266 (20500), 556 (140) |
| [Cu(TE1PA)] ⁺ ^a | 268 (11600), 556 (200) |
| [Cu(CB-TE1PA-trz-prA)] | 277 (19700), 599 (270), 940 (140) |
| [Cu(CB-TE1PA)] ⁺ ^b | 272 (8900), 305 (4300), 600 (230), 938 (150) |

^a From ref. 7a. ^b From ref. 7b.

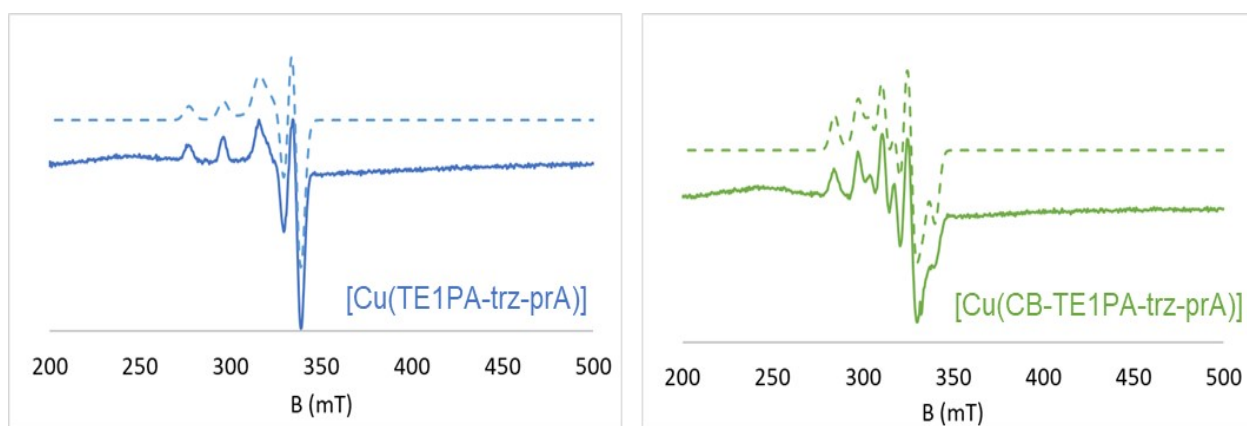


Figure S26. EPR spectra of [Cu(TE1PA-trz-prA)] and [Cu(CB-TE1PA-trz-prA)] complexes. Dashed lines represent the simulated spectra of both complexes.

Table S6. Simulated EPR parameters for [Cu(TE1PA-trz-prA)] and [Cu(CB-TE1PA-trz-prA)] complexes compared to the parent complexes [Cu(TE1PA)]⁺ and [Cu(CB-TE1PA)]⁺ (A_x , A_y and A_z in cm^{-1}).

| | g_x | g_y | g_z | A_x | A_y | A_z |
|--|-------|-------|-------|-------|-------|-------|
| [Cu(TE1PA-trz-prA)] | 2.039 | 2.035 | 2.185 | 2.1 | 45.0 | 192.7 |
| [Cu(TE1PA)] ⁺ ^a | 2.036 | 2.041 | 2.184 | 1.6 | 44.7 | 188.5 |
| [Cu(CB-TE1PA-trz-prA)] | 2.188 | 2.101 | 2.008 | 134.6 | 68.3 | 54.0 |
| [Cu(CB-TE1PA)] ⁺ ^b | 2.192 | 2.108 | 1.987 | 136.3 | 68.1 | 37.7 |

^a From ref. 7a. ^b From ref. 7b.

Kinetic inertness studies

The inertness of the complexes $[\text{Cu}(\text{TE1PA-trz-prA})]$ and $[\text{Cu}(\text{CB-TE1PA-trz-prA})]$ towards acid-assisted dissociation was studied at 25 °C in samples containing 5 M HClO_4 , to allow for direct comparison with the complexes of the parent ligands $[\text{Cu}(\text{TE1PA})]$ and $[\text{Cu}(\text{CB-TE1PA})]$. The vis spectra were run on a PerkinElmer lambda 650 spectrophotometer on Hellma 1400 μL quartz cuvettes with 1 cm optical path. The sample for $[\text{Cu}(\text{TE1PA-trz-prA})]$ was prepared at ca. 1.0 mM directly at the spectrophotometric cuvette and scanned by running spectra at 10 min intervals in the 450–650 nm range. The sample for $[\text{Cu}(\text{CB-TE1PA-trz-prA})]$ was prepared at ca. 0.84 mM in a screw-cap glass culture tube kept tightly closed and incubated at 25 °C during 3 months in a thermostatic incubation bath; sample volumes were taken periodically (once or twice per week) for running spectra in the 450–750 nm range, and then returned to the sample tube. The absorbance of the visible absorption band maximum of each complex (545 or 598 nm) was followed through time and fitted to the observed first order rate constant.

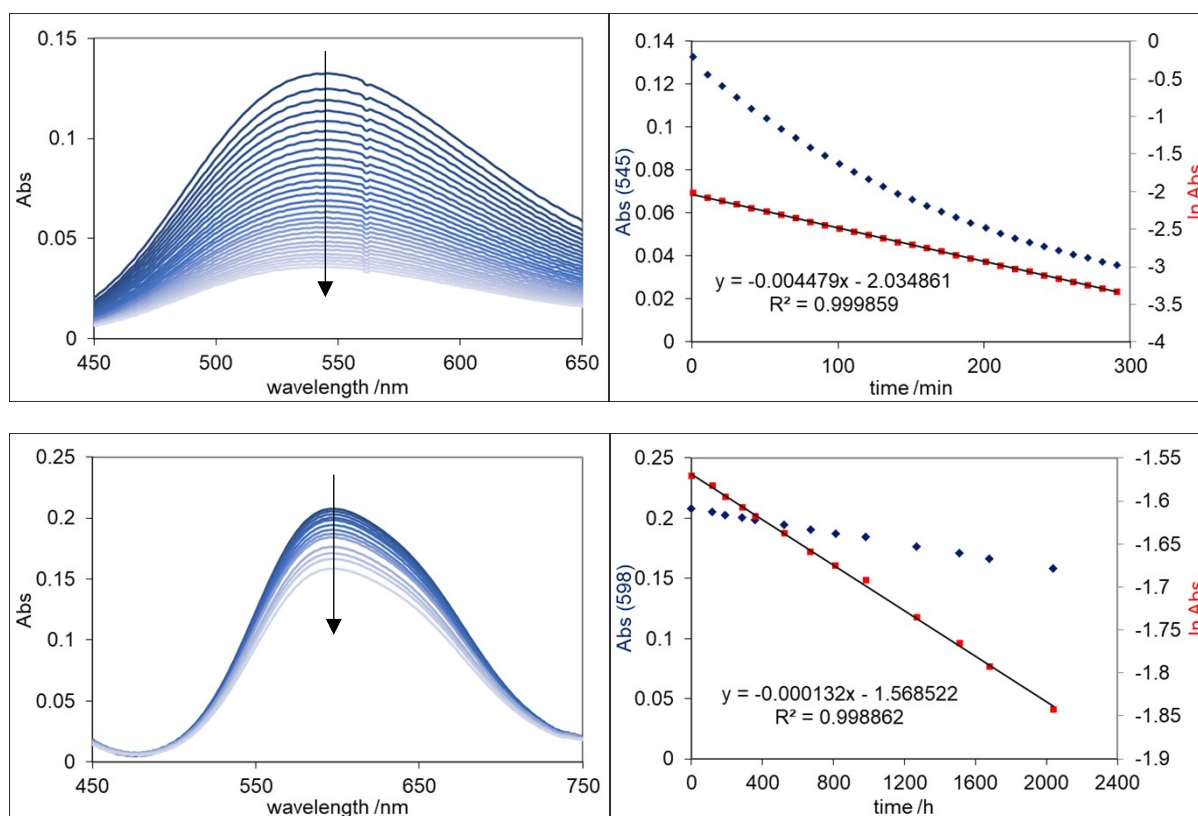


Figure S27. Plots of the acid-assisted dissociation of the complexes $[\text{Cu}(\text{TE1PA-trz-prA})]$ (top) and $[\text{Cu}(\text{CB-TE1PA-trz-prA})]$ (bottom) at 25 °C in 5 M HClO_4 .

Cyclic voltammetry studies

The electrochemistry of the complexes [Cu(TE1PA-trz-prA)] and [Cu(CB-TE1PA-trz-prA)] at neutral pH was studied by cyclic voltammetry in 0.1 M NaClO₄ medium. Cyclic voltammograms were performed in aqueous solution at room temperature (ca. 25 °C) with a BAS CV-50W voltammetric analyzer operated with BAS data acquisition software. Experiments were run in a glass cell BAS MF-1082 placed inside a BAS C-2 cell stand (Faraday cage). The three-electrode setup consisted of a reference Ag/AgCl electrode (BAS MF-2052) filled with aqueous 3 M KCl solution, a platinum wire auxiliary electrode (BAS MW-1032), and a glassy carbon working electrode (BAS MF-2012). Samples of the complexes were prepared at 1.0–1.4 mM in 0.1 M NaClO₄ medium, degassed by bubbling nitrogen prior to all measurements, and kept under a nitrogen stream during the measurements. Between each individual measurement the working electrode was polished on alumina 0.3 μm, cleaned with water and sonicated before use according to standard procedures.⁷ Voltammograms were performed with a sweep rate of 100 mV/s in the region from 0 to –1200 mV, with the voltage being ramped from 0 to –1200 mV and then back to 0 mV, considering the reduction currents as negative. The halfwave potentials, $E_{1/2}$, were calculated by averaging the anodic and cathodic peak potentials. All potential values are reported relative to the Ag/AgCl reference electrode filled with aqueous 3.0 M KCl solution, unless otherwise noted.

Cyclic voltammograms show that [Cu(TE1PA-trz-prA)] has a quasi-reversible reduction system ($E_{1/2}^{\text{red}} = -898$ mV vs Ag/AgCl), while [Cu(CB-TE1PA-trz-prA)] has a reversible one ($E_{1/2}^{\text{red}} = -746$ mV vs Ag/AgCl). Furthermore, both systems are fully stable upon repeated cycling and present reduction peaks at quite negative potentials (E_{pc} of respectively –720 mV and –567 mV vs NHE, upon conversion). This indicates not only that the electrogenerated Cu(I)-complex species are stable on the voltammetry time scale, but also that the reduction potentials are well below the estimated threshold for typical bioreductants (–400 mV vs NHE).

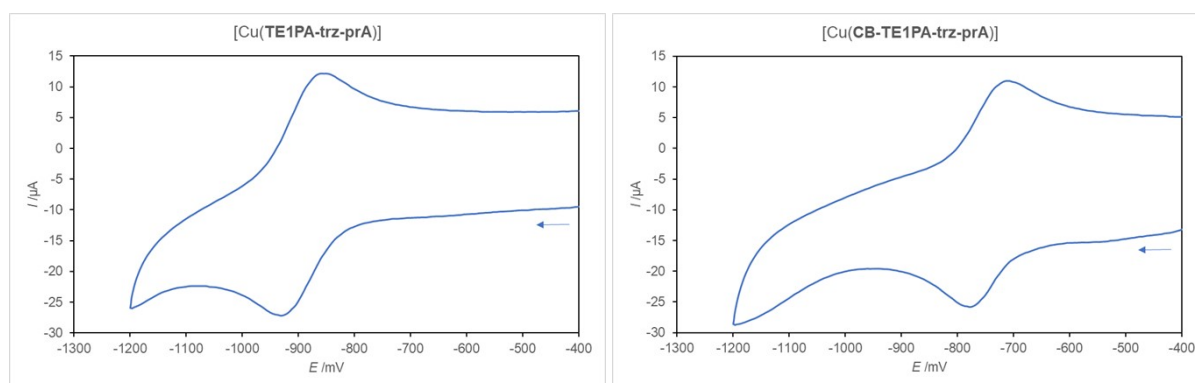


Figure S28. Cyclic voltammograms of the complexes [Cu(TE1PA-trz-prA)] (left) and [Cu(CB-TE1PA-trz-prA)] (right) in aqueous 0.1 M NaClO₄ solution at 100 mV/s scan rate.

Table S7. Cyclic voltammetry parameters of the complexes [Cu(TE1PA-trz-prA)] and [Cu(CB-TE1PA-trz-prA)] obtained in aqueous 0.1 M NaClO₄ solution at 100 mV/s scan rate; values of *E* in mV vs the Ag/AgCl reference electrode filled with aqueous 3.0 M KCl solution, and *I* values in μA.

| Complex | <i>E</i> _{pc} | <i>E</i> _{pa} | <i>I</i> _{pc} | <i>I</i> _{pa} | Δ <i>E</i> _p | <i>I</i> _{pc} / <i>I</i> _{pa} | <i>E</i> _{1/2} ^{red} |
|------------------------|------------------------|------------------------|------------------------|------------------------|-------------------------|---|--|
| [Cu(TE1PA-trz-prA)] | -930 | -866 | -14.99 | 11.47 | 64 | 0.765 | -898 |
| [Cu(CB-TE1PA-trz-prA)] | -777 | -716 | -9.959 | 10.28 | 61 | 1.032 | -746 |

Radiolabeling studies

[⁶⁴Cu]CuCl₂ in 0.1 M HCl was provided by ARRONAX cyclotron (Saint-Herblain, France). For each solution, the copper and total metals concentration was determined by ICP EOS using ICAP PRO XP DUO.

H₂CB-TE1PA-trz-prA: conjugation, radiolabeling and characterization

Two solutions in same MES buffer (50 mM, pH 5) were first prepared: A solution of H₂CB-TE1PA-trz-prA at concentration of 115 μmol/mL (62 mg/mL; 0.0435 mL), and a solution of sulfo-NHS (SNHS) at 575 μmol/mL (125 mg/mL; 0.381 mL). The two solutions were placed in an ice bath. 186 μmol (35.7 mg) EDC was weighed and taken up with 0.324 mL of the sulfo-NHS solution. 0.087 mL (5.01 μmol of sulfo-NHS/EDC) were added to the 0.0435 mL of H₂CB-TE1PA-trz-prA solution, while respecting the molar ratio 1/1/1 ligand/SNHS/EDC, in ice bath for 30 minutes. This activated bifunctional chelator reacted with the antibody without further purification. The coupling reaction was performed with a ligand to antibody ratio of 10, 20, 50, 100 and 200 equivalents, by mixing a calculated volume of the activated ligand solution with a solution of 1 mg (6.67 nmol) of hLL2 antibody (4.2 mg/mL; 28 nmol/mL) in carbonate buffer (0.3 M pH 8.6). The reaction mixture was stirred at room temperature overnight. The coupling reactions performed with 50 and more equivalents showing protein precipitation, only the experiments with 10 and 20 equivalents were further considered. The excess of ligand was removed by gel filtration using a desalting Nap-5 column (cut off 10 kDa) and 0.1 M sodium acetate buffer (pH 6) in order to avoid future antibody buffer change. The fractions of interest were brought together and concentrated. The concentration of the solution was measured by UV-visible spectrophotometry at 280 nm (Nanodrop™ spectrometer). To estimate the percentage of aggregate generated by the coupling process, the conjugates were analyzed with an UHPLC system (UHPLC HClass bio Waters with Empower pro 1154 software; Protein BEH SEC column (1.7μ, 4.6 × 150 mm); Solvent: PBS with a flow rate of 0.4 mL/min).

The number of coupled chelates per antibody, and by extension the yield of the coupling reactions, was evaluated by a copper-64 test labelling. The tests were performed as follows: [⁶⁴Cu]CuCl₂ (Volume activity: 2570 MBq/mL; Copper concentration: 45.04 pmol/μL; Total metals: 84.56 pmol/μL) in 0.1 M HCl solution was first buffered at pH 6 by addition of 10% (Volume/Volume) of 2.5 M sodium acetate. The purified conjugated antibody was then added to a known amount of buffered copper solution, in order to obtain a total copper-to-antibody molar ratio of 5 and 10. The mixture was incubated at 40 °C for 30 min. Then, a calculated volume of 1 mM EDTA was added to the radiolabeling solution (EDTA final concentration: 0.01 mM) to complex free [⁶⁴Cu]-nuclide. The mixture was stirred at room temperature for 5 min. The radiochemical purity was evaluated with an instant Thin Layer Chromatography plate (Agilent Technologies) with 0.1 M sodium citrate buffer (pH 4.5) as eluent. After

development, the plate was exposed on a storage phosphor screen, which was revealed using a Cyclone[®] Plus phosphor imager (Perkin Elmer). The radiolabeled antibody conjugate stays at the bottom ($R_f = 0$) while the $[^{64}\text{Cu}(\text{EDTA})]^{2-}$ migrates to the top of the plate ($R_f = 1$). The number of chelates grafted to the antibody was calculated using the following formula: the number of chelates per antibody is equal to the total amount (nmol) of copper added multiplied by the percentage of radioactivity bound to the antibody (radioactivity at $R_f = 0$) divided by the amount of antibody (nmol) used for the assay.

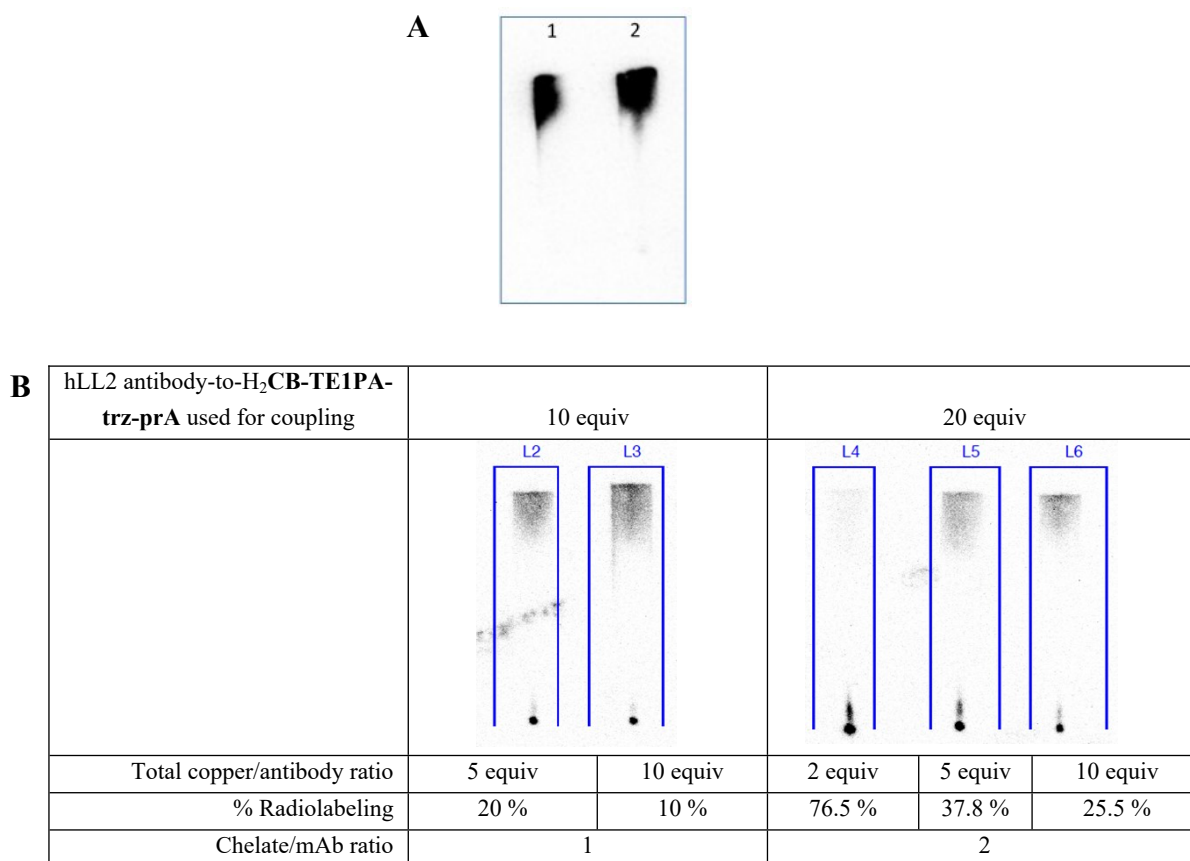


Figure S29. Optimization of the conjugation on the hLL2 antibody by TLC. A) References: 1: $[^{64}\text{Cu}(\text{EDTA})]^{2-}$ and 2: non coupled hLL2 antibody with $[^{64}\text{Cu}]$ -nuclide. B) Determination of the number of chelates per hLL2 antibody.

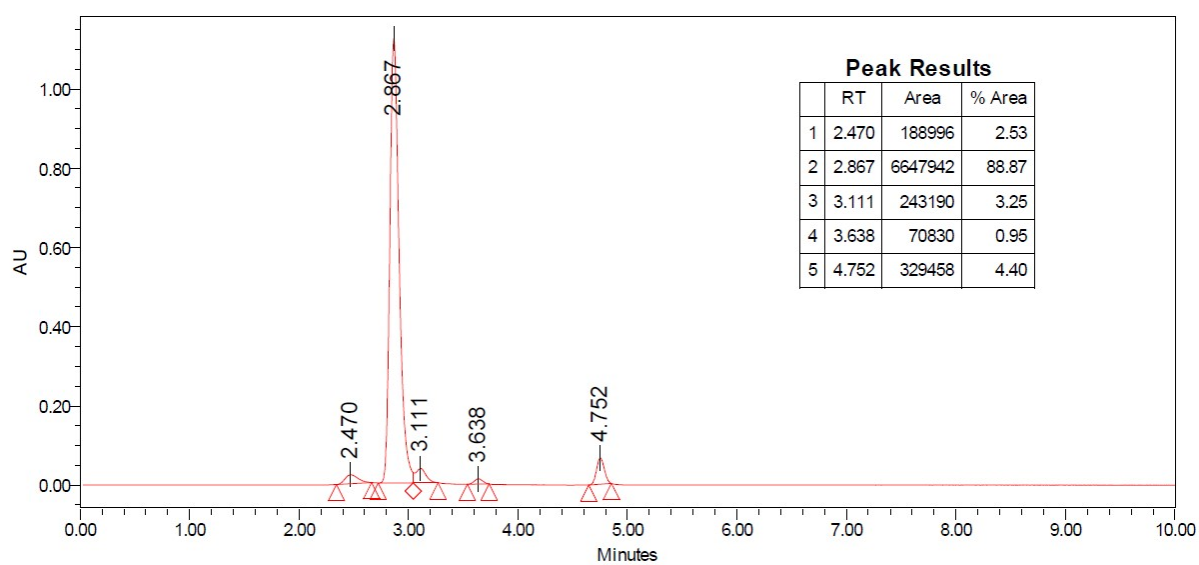
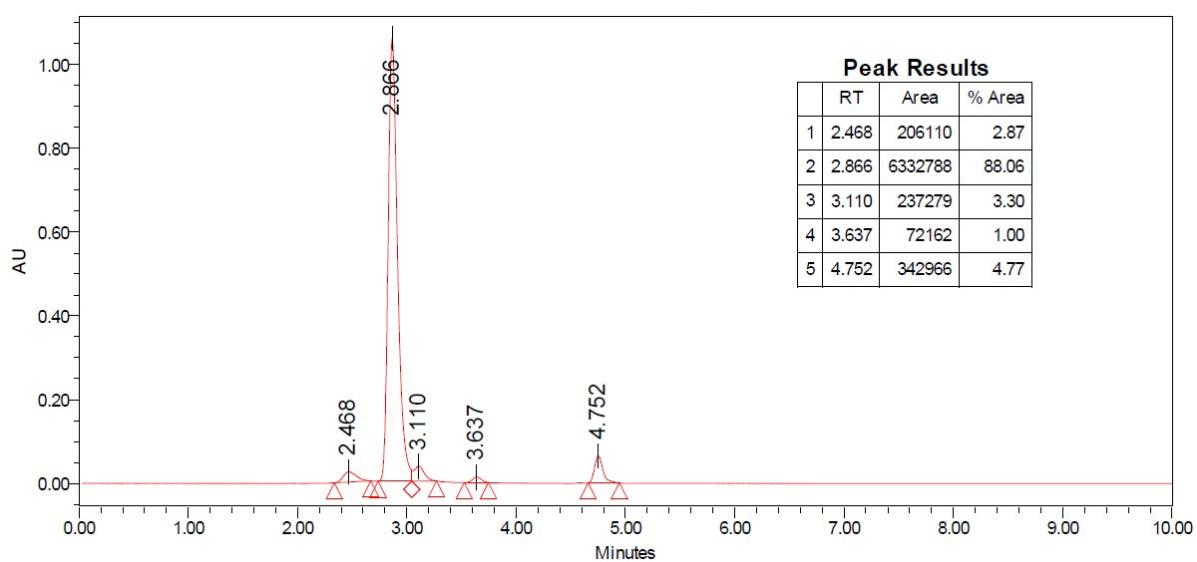
A**B**

Figure S30. HPLC profiles of the hLL2 antibody conjugated with the bifunctional chelator H₂CB-TE1PA-trz-prA. A) hLL2 antibody-to-H₂CB-TE1PA-trz-prA = 10 equiv; B) hLL2 antibody-to-H₂CB-TE1PA-trz-prA = 20 equiv.

Radiolabeling of H₂TE1PA-trz-prA.4HCl

[⁶⁴Cu]CuCl₂ in 0.1 M HCl (23.1 μL, 180 pmol Cu, 767.4 pmol total metals) was buffered with 3 μL of 2.5 M sodium acetate. Radiolabeling was then performed by mixing the buffered solution of [⁶⁴Cu]CuCl₂ with 5.2 μL of H₂TE1PA-trz-prA.4HCl at 0.38 mg/mL in 0.1 M HCl (100 μg, 172 nmol) and then completed with 27.5 μL of 0.1 M sodium acetate to adjust the pH close to 6. The mixture was incubated at 42 °C for 30 min. A 100-fold EDTA (1 mM pH 6 in water) to ligand excess was then added to complex the potential remaining free copper. Radiochemical purity of [⁶⁴Cu][Cu(TE1PA-trz-prA)] complex was controlled with two systems. Firstly, TLC analysis was performed using silica gel on TLC-PET foils (Merck) and the eluent used was a mixture of ammonium chloride (20% in water) and methanol (1:1). Secondly, an aliquot of 20 μL radiolabeled solution was injected into the radio-HPLC system consisting of an Eckert & Ziegler HPLC module, Eckert & Ziegler detector shielding module, Modular-Lab software and ACE C18 column (3 μm, 150 × 3 mm). The elution gradient applied to HPLC system was 10% to 100% enrichment of acetonitrile with 0.05% trifluoroacetic acid in 15 min with a flow rate of 0.4 mL/min. Chromatogram was analyzed with Modular-Lab software by integration of the areas under the curve (AUC) of each peak. Radiochemical purity corresponds to the AUC of interest peak divided by the sum of the total AUCs detected. The radiolabeling yield was found to be greater than 99% (molar activity: 240 kBq/nmol; radiochemical purity: 99%).

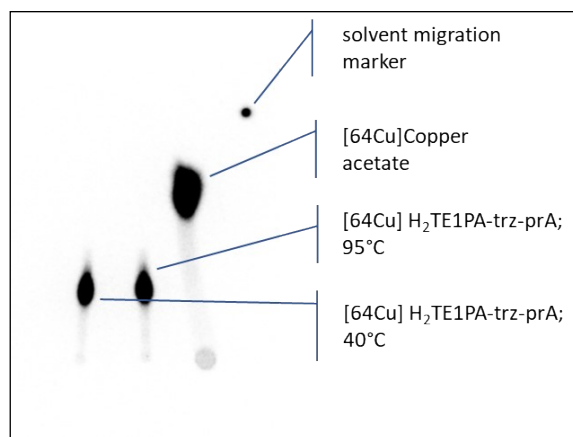


Figure S31. TLC-PET analysis after ⁶⁴Cu-labeling of H₂TE1PA-trz-prA (2.5 M sodium acetate, pH = 5-6, 30 min, 42 °C).

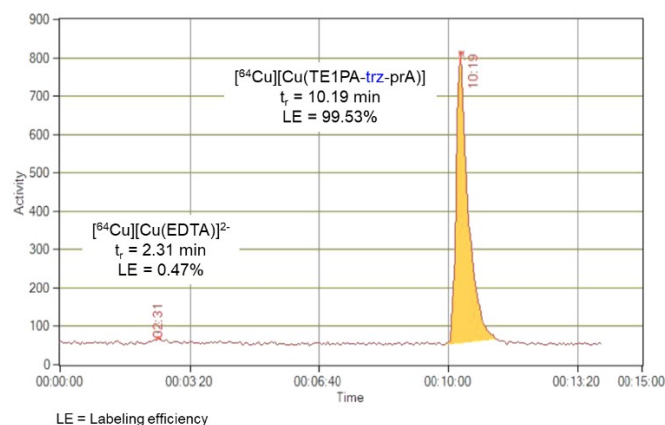


Figure S32. HPLC-radiochromatogram after ^{64}Cu -labeling of $\text{H}_2\text{TE1PA-trz-prA}$ (2.5 M sodium acetate, pH = 5-6, 30 min, 42 °C).

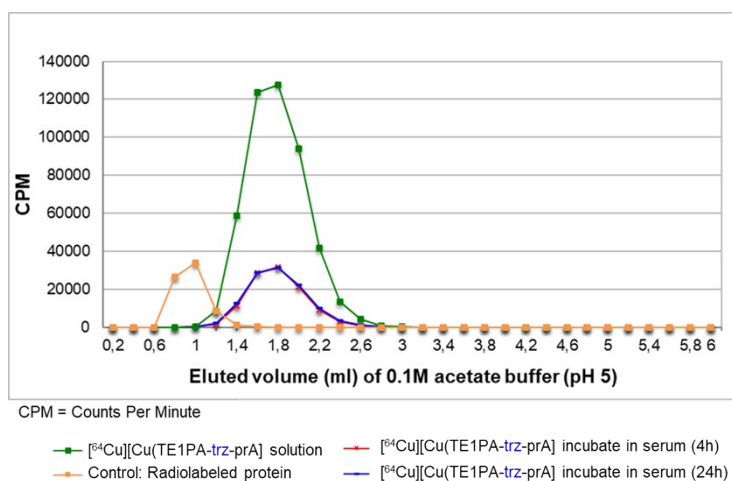


Figure S33. Gel filtration analysis of serum incubated with $[^{64}\text{Cu}][\text{Cu}(\text{TE1PA-trz-prA})]$ at 37 °C over 24 h.

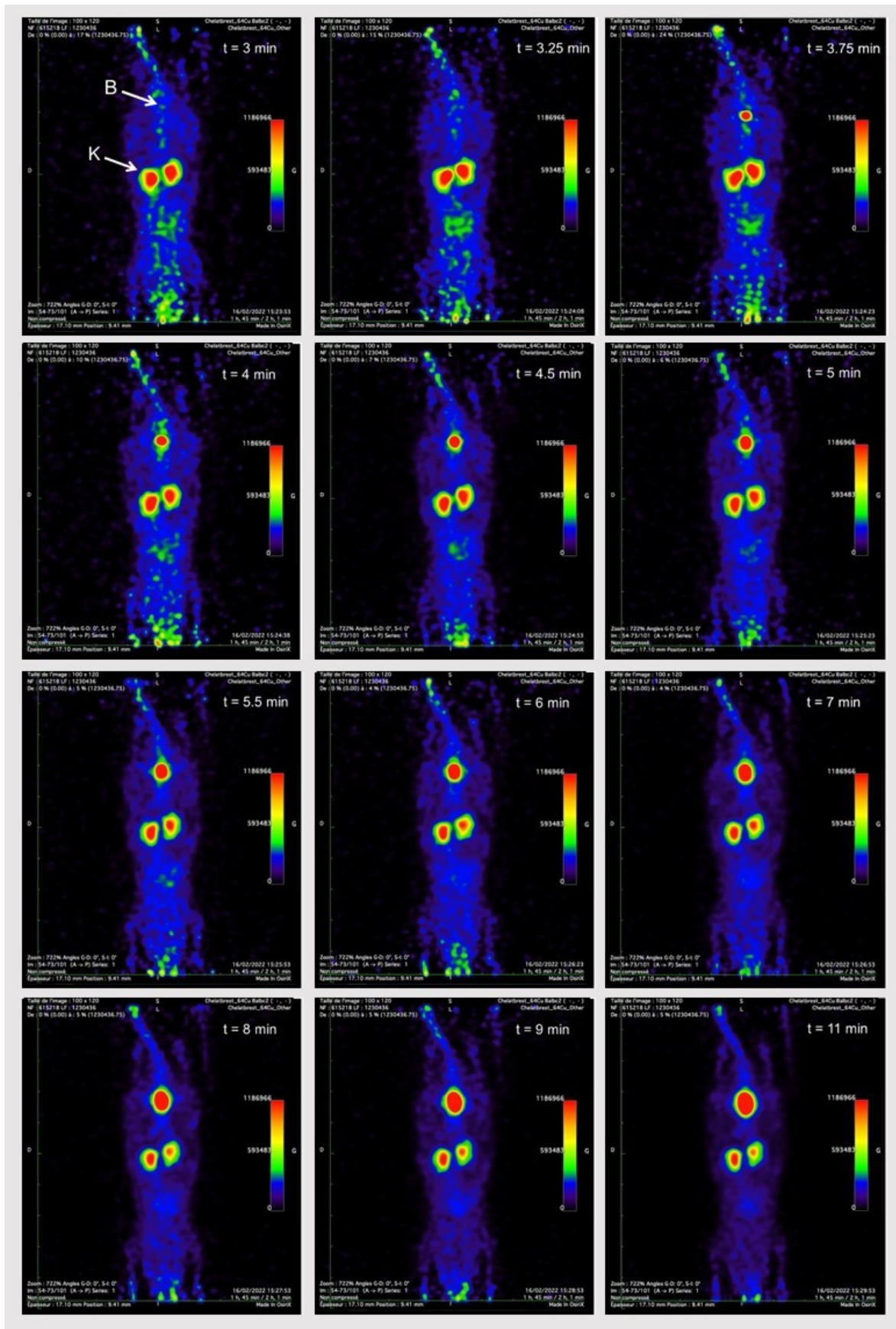
***In vivo* studies with $[^{64}\text{Cu}][\text{Cu}(\text{TE1PA-trz-prA})]$ and micro-PET imaging**

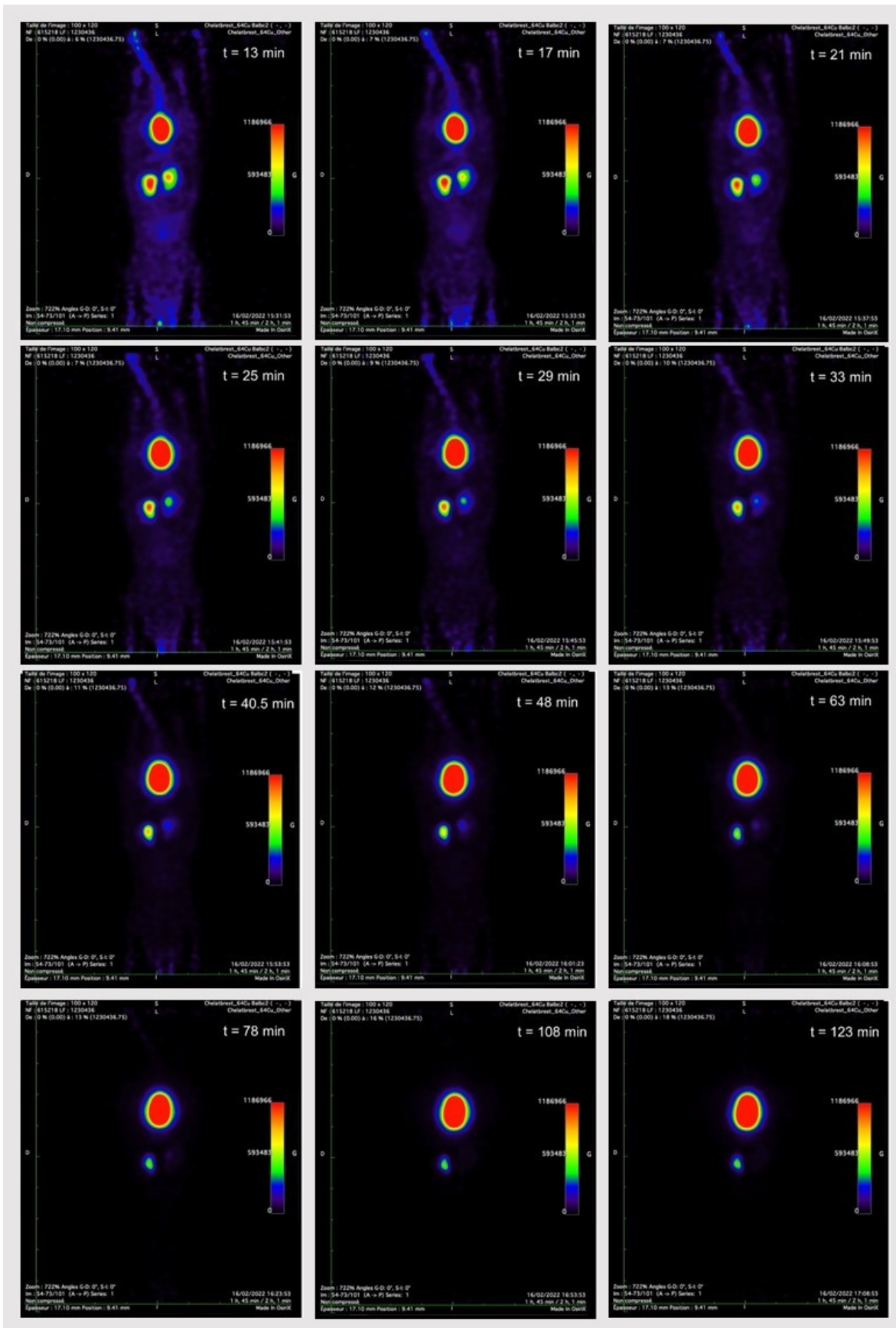
$[^{64}\text{Cu}][\text{Cu}(\text{TE1PA-trz-prA})]$ biodistribution studies were performed on 12 female BALB/c mice of 9 weeks old (Referral: 22764. Accommodation number: 2022-032). PET imaging was performed on 3 mice at 24 h and 48 h post injection of 8 MBq $[^{64}\text{Cu}][\text{Cu}(\text{TE1PA-trz-prA})]$ (20 μg). After imaging, this group has been sacrificed by anesthesia and cervical dislocation. 9 mice were used for the biodistribution study. 3 mice per timepoint at 2 h, 24 h and 48 h post-injection of 3 MBq $[^{64}\text{Cu}][\text{Cu}(\text{TE1PA-trz-prA})]$ radiochelate (20 μg) were killed and dissected. Each relevant organ was dried, weighed and placed in a plastic tube that was then counted using a well gamma counter. For the liver study, a hepatic lobe was washed out with 0.9% NaCl at 4 °C and then kept on ice in a tube containing a 0.1 M solution of

ethanol/ammonium acetate (65:35) and a protease inhibitor cocktail. The liver sample was then destroyed with potter to obtain a homogeneous suspension that was centrifugated at 8000 g during 30 min at 4 °C using a 2-16PK centrifuge (Sigma). Precipitate and supernatant were separated and counted with a gamma counter. Then the supernatant was analyzed by radio HPLC system with a stacked 12 10/300 GL column. The run was in isocratic mode at 0.5 mL/min flow during 60 min and the elution solvent was a mixture of 200 mM HEPES and 150 mM NaCl pH 7.3.

Dynamic imaging study was performed [⁶⁴Cu][Cu(**TE1PA-trz-prA**)] on one female BALB/c mouse of 11 weeks old (Referral: 22764. Accommodation number: 2022-032. Pet store approval: C44-278). Images acquisition was performed 3 min after injection of 3.3 MBq (100 µL) [⁶⁴Cu][Cu(**TE1PA-trz-prA**)] (20 µg) into the tail mouse vein. Before being positioned in the micro-PET equipment, the animal was placed in an induction box and anesthetized with 4% isoflurane. Once asleep, the animal was placed in the imaging cell with its head contained in a mask directly connected to the anesthesia station in order to ensure a continuous flow of isoflurane at 1.5% during the acquisition. Conservation of body temperature during acquisition was maintained *via* a forced air circulation system through thin channels integrated into the bed of the imaging cell. The deposit of a drop of ocrygel on the eyes of the mouse was done to protect the eyes from drying out.

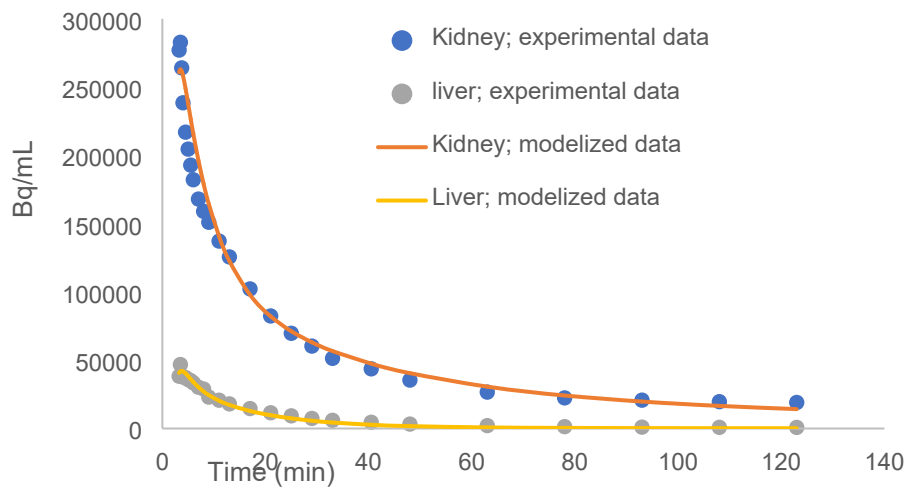
Mouse was imaged on a PET/CT IRIS (INVISCAN) equipment at the CIMA platform (CHU, Nantes, France) that presents the followed characteristics: Sensitivity > 9% [250–750 keV], Spatial resolution = 1.1 mm (radiolabeling EM.), Axial field of view: > 94 mm (Recon FOV = 102.6 mm), Transverse field of view: ~ 81 mm, Energy resolution: < 13%. Time resolution = 1.8 ns. Dynamic images acquisition was maintained during to 2 h with 24 frames: 3, 3.25, 3.75, 4, 4.5, 5, 5.5, 6, 7, 8, 9, 11, 13, 17, 21, 25, 29, 33, 40.5, 48, 63, 78, 108, 123 minutes post injection. Treatment (reconstruction and analyses) of each image was performed using OsiriX software.





Fi

Figure S34. Dynamic micro-PET images of BALB/c mouse from $t = 3$ min to 123 min post-injection following injection with $[^{64}\text{Cu}][\text{Cu}(\text{TE1PA-trz-prA})]$ (K: kidneys; B: bladder).



| Pharmacokinetic parameters | | | | |
|----------------------------|-------------------------|-------------------------|----------|----------|
| | K1 (min ⁻¹) | K2 (min ⁻¹) | T1 (min) | T2 (min) |
| Liver | -0,023 | -0,105 | 29,949 | 6,609 |
| Kidneys | -0,011 | -0,098 | 62,982 | 7,035 |

Figure S35. Pharmacokinetic curves of liver and kidneys and associated constants extrapolated from dynamic micro-PET images.

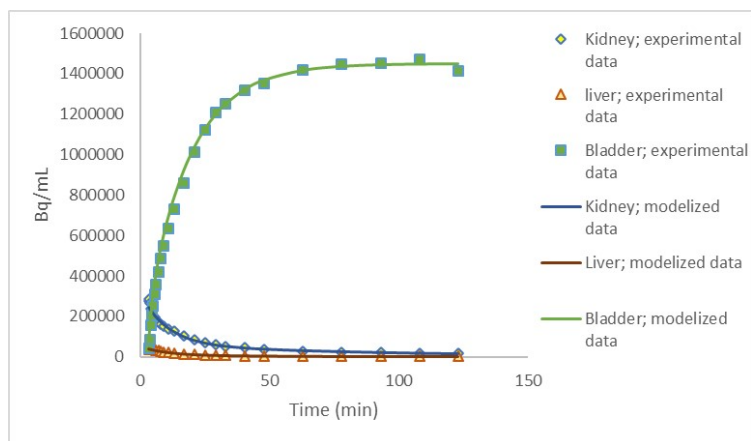


Figure S36. Pharmacokinetic curves of bladder compared to liver and kidneys extrapolated from dynamic micro-PET images.

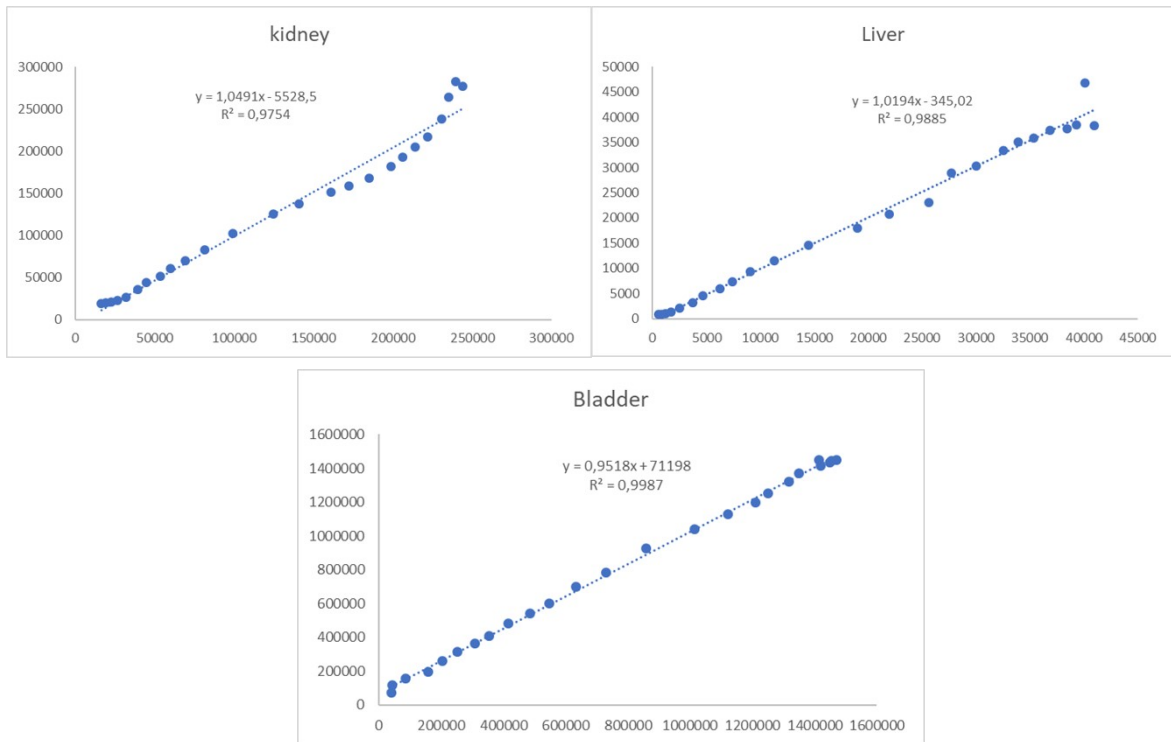


Figure S37. Goodness of fit using a plot between observed and calculated results of biodistribution in kidneys, liver and bladder.

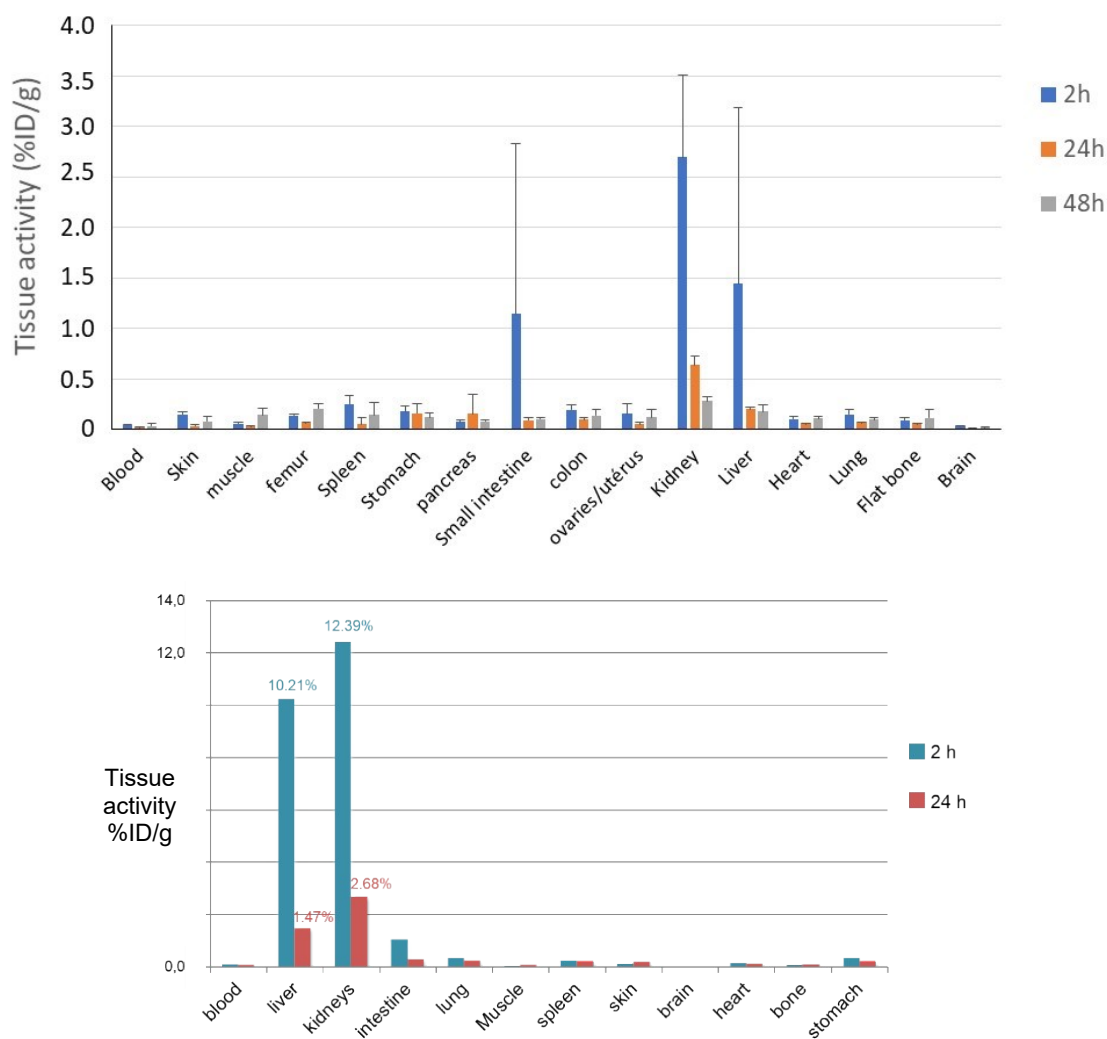


Figure S38. Biodistribution of, up: $[^{64}\text{Cu}][\text{Cu}(\text{TE1PA-trz-prA})]$ in BALB/c mice at 2 h, 24h and 48 h from this paper and, bottom: $[^{64}\text{Cu}][\text{Cu}(\text{TE1PA})]^+$ in BALB/c mice at 2 h and 24 h from the literature¹⁷

For the *ex vivo* biodistribution, organs and blood from mice were collected at 2 h, 24 h, and 48 h post-injection of $[^{64}\text{Cu}][\text{Cu}(\text{TE1PA-trz-prA})]$ and the associated radioactivity was analyzed by a gamma counter. Processing of the resulting data allowed for determination of the % ID/g of each organ leading to the biodistribution profile at the three time points (Figure 4, Table 2). A very low percentage of radioactivity (< 0.25 % ID/g) was measured in almost all organs and blood at 2 h post-injection except, logically, in the usual critical organs: small intestine, liver, and especially kidneys due to renal elimination. The highest uptake was observed in the kidneys with 2.69% ID/g while the small intestine and liver showed percentages of 1.14% ID/g and 1.44% ID/g respectively; however, these values are particularly low compared to the usual distribution of such non-conjugated radiocomplexes. Even better, at 24 h post-injection, the activity found in these three organs becomes almost insignificant

considering the uncertainty at this low % ID/g. Indeed, the measurements indicated a remarkable clearance of the [^{64}Cu][Cu(**TE1PA-trz-prA**)] radiocomplex after 24 h with a residual activity of 0.20% ID/g in the liver and 0.64% ID/g in the kidneys. In comparison, the biodistribution profile previously obtained with the [^{64}Cu][Cu(**TE1PA**)]⁺ complex (Figure S38) revealed a significant higher uptake in the kidneys (12.39% ID/g) and liver (10.21% ID/g) at 2 h post-injection, while the remaining activity at 24 h for [^{64}Cu][Cu(**TE1PA**)]⁺ was almost the same as that found for [^{64}Cu][Cu(**TE1PA-trz-prA**)] at 2 h. These values are 5 to 7 times higher than those found for [^{64}Cu][Cu(**TE1PA-trz-prA**)]. Remarkably, **HTE1PA** had already outperformed other ^{64}Cu -radiocomplexes such as those obtained with DOTA in comparable *in vivo* studies,⁷ indicating the significance of the further improvement on biodistribution for the [^{64}Cu][Cu(**TE1PA-trz-prA**)] complex.

References

1. S. Stoll, A. Schweiger, *J. Magn. Reson.*, 2006, **178**, 42–55.
2. F. Molton, *Magn. Reson. Chem.*, 2020, **58**, 718–726.
3. A. Bourdolle, M. Allali, J.-C. Mulatier, B. Le Guennic, J. M. Zwier, P. L. Baldeck, J.-C. G. Bünzli, C. Andraud, L. Lamarque, O. Maury, *Inorg. Chem.*, 2011, **50** (11), 4987–4999.
4. R. N. Murugan, J.-E. Park, D. Lim, M. Ahn, C. Cheong, T. Kwon, K.-Y. Nam, S. H. Choi, B. Y. Kim, Yoon, M. B. Yaffe, D.-Y. Yu, K. S. Lee, J. K. Bang, *Bioorg. Med. Chem.*, 2013, **21** (9), 2623–2634.
5. L. A. Galán, N. Hamon, C. Nguyen, E. Molnár, J. Kiss, J. Mendy, K. Hadj-Kaddour, M. Onofre, G. Trencsényi, C. Monnereau, M. Beyler, G. Tircsó, M. Gary-Bobo, O. Maury, R. Tripier, *Inorg. Chem. Front.*, 2021, **8** (9), 2213–2224.
6. T. Storr, B. R. Cameron, R. A. Gossage, H. Yee, R. T. Skerlj, M. C. Darkes, S. P. Fricker, G. J. Bridger, N. A. Davies, M. T. Wilson, K. P. Maresca, J. Zubieta, *Eur. J. Inorg. Chem.*, 2005, **13**, 2685–2697.
7. a) L. M. P. Lima, D. Esteban-Gómez, R. Delgado, C. Platas-Iglesias, R. Tripier, *Inorg. Chem.*, 2012, **51**, 6916–6927; b) L. M. P. Lima, Z. Halime, R. Marion, N. Camus, R. Delgado, C. Platas-Iglesias, R. Tripier, *Inorg. Chem.*, 2014, **53** (10), 6916–5927.
8. R. Delgado, M. C. Figueira, S. Quintino, *Talanta* 1997, **45**, 451–462.
9. R. F. Jameson, M. F. Wilson, *J. Chem. Soc., Dalton Trans.*, 1972, 2607–2610.
10. P. Gans, A. Sabatini, A. Vacca, *Talanta*, 1996, **43**, 1739–1753.
11. L. Alderighi, P. Gans, A. Ienco, D. Peters, A. Sabatini, A. Vacca, *Coord. Chem. Rev.*, 1999, **184**, 311–318.

12. G. M. Sheldrick, *Acta Cryst.*, 2015, A71, 3-8.
13. G. M. Sheldrick, *Acta Cryst.*, 2015, C71, 3-8.
14. L. Yang, D. R. Powel, R. P. Houser, *Dalton Trans.*, 2007, **9**, 655-964.
15. X. Liang, P. J. Sadler, *Chem. Soc. Rev.*, 2004, **33**, 246–266.
16. J. Dale, *Acta Chem. Scand.*, 1973, **27**, 1115–1129.
17. M. Frindel, N. Camus, A. Rauscher, M. Bourgeois, C. Alliot, L. Barré, J. F. Gestin, R. Tripier, A. Faivre-Chauvet, *Nucl. Med. Biol.*, 2014, e49-57.